

DIRECTIONS AND RATES OF GROUND-WATER MOVEMENT IN THE VICINITY OF  
KESTERSON RESERVOIR, SAN JOAQUIN VALLEY, CALIFORNIA

By R.J. Mandle and A.L. Kontis

---

U.S. GEOLOGICAL SURVEY

Water-Resources Investigations Report 86-4196

REGIONAL AQUIFER SYSTEMS ANALYSIS

Prepared in cooperation with the

U.S BUREAU OF RECLAMATION

6439-11



Sacramento, California  
1986

UNITED STATES DEPARTMENT OF THE INTERIOR

DONALD PAUL HODEL, Secretary

GEOLOGICAL SURVEY

Dallas L. Peck, Director

---

For additional information write to:

District Chief  
U.S. Geological Survey  
Federal Building, Room W-2234  
2800 Cottage Way  
Sacramento, CA 95825

Copies of this report  
may be purchased from:

U.S. Geological Survey  
Books and Open-File Reports  
Box 25425  
Building 41, Federal Center  
Denver, CO 80225  
Telephone: (303) 236-7476

## CONTENTS

	Page		Page
Abstract .....	1	Model design and development--Continued	
Introduction .....	2	Estimation of specific yield .....	16
Well-numbering system .....	2	Boundary conditions .....	16
Description of study area .....	3	Head dependent ground-water	
Geology .....	3	sources and sinks .....	18
Ground-water hydrology .....	5	Rivers, sloughs, and canals .....	18
Modeling ground-water flow .....	9	Duck ponds .....	19
Governing equation .....	9	Kesterson Reservoir .....	19
Boundary conditions .....	9	Evapotranspiration .....	20
Head dependent ground-water		Model simulations .....	20
sources and sinks .....	9	Simulation of steady-state	
Numerical methods .....	13	winter-spring flow conditions ...	21
Model design and development .....	13	Three-year transient simulation ...	28
Finite-difference grid .....	13	Simulation of summer-fall	
Estimation of vertical hydraulic		flow conditions .....	34
conductivity for streambeds,		Estimating ground-water flow	
canals, and pond bottoms .....	13	direction and traveltime .....	40
Estimation of horizontal and		Model limitations .....	46
vertical hydraulic conductivity		Summary and conclusions .....	47
for model layers 1, 2, and 3 ....	15	Selected references .....	48
Estimation of vertical hydraulic		Appendix A: Calculating	
conductivity for E clay .....	16	travel distances .....	50

## ILLUSTRATIONS

	Page
Figure 1. Map showing location of study area.....	4
2-3. Maps showing water-level contours for the shallow aquifer in the vicinity of Kesterson Reservoir:	
2. January 1985 .....	6
3. August 1985 .....	7
4. Hydrograph showing water levels measured in well 8S/10E-21L4M, 1950-85 .....	8
5-7. Diagrams showing:	
5. Model representation of a duckpond or river .....	10
6. Diagram showing head dependent ground-water source or sink function .....	11
7. Diagram showing evapotranspiration as a function of head in the aquifer .....	12
8. Map showing finite-difference grid used in model .....	14
9-10. Maps showing hydraulic heads in model layer 1 for winter-spring flow conditions using:	
9. High values of hydraulic conductivity .....	22
10. Low values of hydraulic conductivity .....	23
11. Map showing location of wells measured by the U.S. Bureau of Reclamation .....	27

	Page
Figure 12. Hydrographs showing comparison of measured and simulated hydraulic heads for selected observation wells, May 1982 to March 1985 .....	29
13-14. Maps showing simulated hydraulic heads in model layer 1 for summer-fall flow conditions using:	
13. High values of hydraulic conductivity .....	35
14. Low values of hydraulic conductivity .....	36
15. Map showing directions and rates of ground-water flow from Kesterson Reservoir along selected flow paths .....	42
16. Graphs showing travel distances along flow paths 1 through 12 .....	43
17. Diagrams showing relation of volumetric fluxes to finite-difference block faces and finite-difference nodes .....	51
18. Diagrams showing transformation of a rectangle in the x,y,z coordinate system into a cube in the isoparametric coordinate system .....	53

---

TABLES

---

	Page
Table 1. Values of horizontal (Kh) and vertical (Kv) hydraulic conductivity used in model simulations .....	15
2. Average ground-water flow rates for each model boundary .....	17
3. Measured hydraulic heads in piezometers above and below E clay .....	17
4. Average water levels in Kesterson Reservoir ponds used for winter-spring and summer-fall simulations .....	20
5. Comparison of simulated winter-spring hydraulic heads with measured hydraulic heads averaged for winter and spring months, May 1982 to March 1985 .....	24
6. Comparison of simulated summer-fall hydraulic heads with measured hydraulic heads averaged for summer and fall months, May 1982 to March 1985 .....	37

## CONVERSION FACTORS

For this report, the inch-pound system of units was used. For those readers who may prefer metric (International System) units rather than inch-pound units, the conversion factors for the terms used in this report are listed below:

<u>Multiply inch-pound unit</u>	<u>By</u>	<u>To obtain metric unit</u>
acres	4,047	square meters
acre-ft (acre-feet)	1,233	cubic meters
ft (feet)	0.3048	meters
ft/d (feet per day)	0.3048	meters per day
ft <sup>3</sup> /s (cubic feet per second)	0.0283	cubic meters per second
ft/s (feet per second)	0.3048	meters per second
ft/yr (feet per year)	0.3048	meters per year
inches	25.4	millimeters
in/yr (inches per year)	25.4	millimeters per year
mi (miles)	1.609	kilometers
mi <sup>2</sup> (square miles)	2.590	square kilometers

DIRECTIONS AND RATES OF GROUND-WATER MOVEMENT IN THE VICINITY OF  
KESTERSON RESERVOIR, SAN JOAQUIN VALLEY, CALIFORNIA

---

By R.J. Mandle and A.L. Kontis

---

ABSTRACT

A three-dimensional ground-water flow model was used to simulate ground-water flow for a 124 square-mile area in the vicinity of Kesterson Reservoir in the San Joaquin Valley, California. Available data were used to calculate a probable range of ground-water flow rates, but calibration and sensitivity analysis were not done for this model.

Flow directions, as inferred from measured ground-water levels and simulated hydraulic heads from all model simulations, indicate that regional ground-water flow is from the south to north. Kesterson Reservoir acts as a recharge mound superimposed on the regional-flow system. Ground water moves in the horizontal and vertical direction away from Kesterson Reservoir. Mud and Salt Sloughs act as ground-water discharge areas. Simulated ground-water

flow from Kesterson Reservoir did not flow beyond these sloughs. Ground water from west of Mud Slough seems to flow west toward Los Banos Creek and east toward Mud Slough. Ground water that travels toward Salt Slough from Kesterson Reservoir probably is lost by evapotranspiration near the surface before reaching Salt Slough. Ground water between Salt Slough and the San Joaquin River seems to flow north and toward Salt Slough and the San Joaquin River. The canals and duck ponds generally act as sources of ground-water recharge.

A method was developed for determining flow directions and distance traveled in three dimensions for discrete time increments using simulated ground-water fluxes. Simulated average horizontal pore velocities away from Kesterson range from less than 0.01 to 140 feet per year. The simulated average vertical pore velocities range from 0.01 to 14.7 feet per year.

## INTRODUCTION

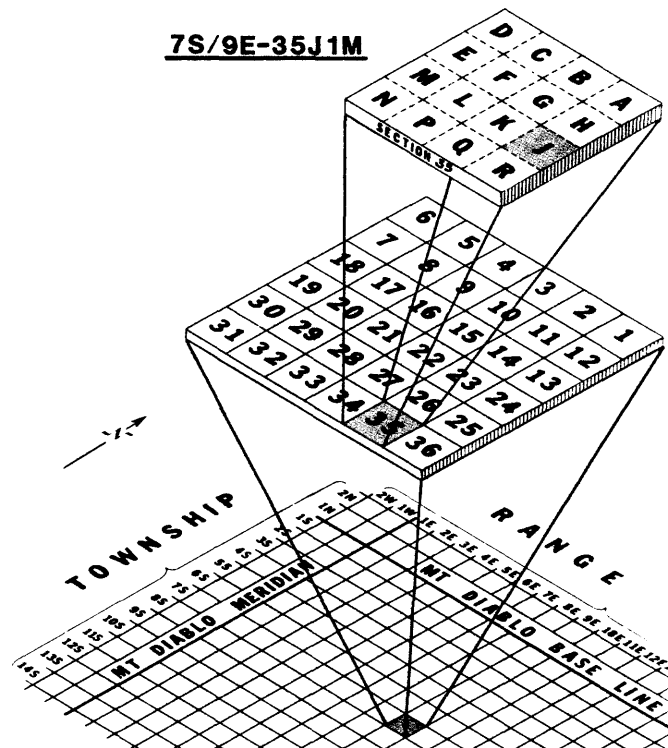
Kesterson Reservoir consists of a series of 12 evaporation ponds that are used to store agricultural drainage water. The agricultural drainage water is from subsurface tile drains that carry irrigation-return flow from about 8,000 acres of farmland. The drainage water contains high levels of salts and trace elements, particularly selenium, which has caused high incidences of mortality and birth defects in waterfowl at Kesterson Reservoir (U.S. Bureau of Reclamation, 1984). Drainage water that seeps from Kesterson Reservoir to underlying ground water is of concern because of possible contamination of nearby domestic wells or surface water, including the San Joaquin River.

The purpose of this study was to characterize the ground-water flow system in the vicinity of Kesterson Reservoir using existing data. The approach used was to develop a three-dimensional ground-water flow model to simulate hydraulic heads and rates and directions of ground-water flow. Such a model is a useful tool for extracting as much information as possible on the ground-water flow system from data that are already available and do not require costly field investigations to collect. The data available for the study, however, were not sufficient to allow for model calibration and verification, or detailed sensitivity analysis. Thus, the model developed and described in this study is a first approximation of the ground-water flow system in the vicinity of Kesterson Reservoir and is not intended for quantitative predictions. This study is one of a series of hydrologic investigations of the San Joaquin Valley being done by the U.S. Geological Survey, in cooperation with the U.S. Bureau of Reclamation, and as part of the U.S. Geological Survey Regional Aquifer Systems Analysis (RASA) program. These investigations focus on assessing the sources, distribution, movement, and fate

of selenium and other trace elements in the hydrologic system of the San Joaquin Valley, particularly the western part.

## WELL-NUMBERING SYSTEM

Wells are identified according to their location in the rectangular system for the subdivision of public lands. Their identification consists of the township number, north or south; the range number, east or west; and the section numbers. Each section is further divided into sixteen 40-acre tracts lettered consecutively (except I and O), beginning with A in the northeast corner of the section and progressing in a sinusoidal manner to R in the southeast corner. Within the 40-acre tract, wells are sequentially numbered in the order they are inventoried. The final letter in a well identification number refers to the base line and meridian. All wells in the study area are referenced to the Mount Diablo base line and meridian (M). The illustration below shows how the well number 7S/9E-35J1M is derived.



## DESCRIPTION OF STUDY AREA

Kesterson Reservoir is in the Kesterson National Wildlife Refuge on the west side of the San Joaquin Valley, California (fig. 1). The wildlife refuge is east of the city of Gustine, and west of the San Joaquin River. This area lies on the flood plain of the San Joaquin River and is subject to infrequent flooding. The study area has a flat topography ranging in altitude from less than 60 to 90 feet. Remnants of the meandering San Joaquin River and its tributaries traverse this area in many places. Kesterson Reservoir is bordered by two tributaries of the San Joaquin River. Mud Slough is on the immediate west side and Salt Slough is 1 to 2 miles to the east. The San Joaquin River lies beyond Salt Slough, another 1 to 2 miles to the east.

The study area has very hot, dry summers and mild, damp winters. The San Joaquin Valley is in the rain shadow of the Coast Ranges and because of this, annual precipitation averages only 10 to 15 inches. Most of this precipitation occurs during the winter months. The estimated pan evaporation from pastureland near Kesterson Reservoir was 52.5 inches per year (California Department of Water Resources, written commun., 1967). Most of this evaporation takes place during the summer months and decreases substantially during the winter.

### Geology

Continental rocks and deposits of Quaternary and Tertiary age derived from the Coast Ranges and Sierra Nevada make up the bulk of the valley-fill material in the San Joaquin Valley. These deposits range in thickness from virtually 0 to about 3,000 feet (Hotchkiss and Balding, 1971, pl. 1, and Miller and others, 1971, pl. 4). The Tertiary sediments are predominately alluvial-fan, flood-plain, river-channel, lacustrine,

and marsh deposits. These types of deposits consist of sand, gravel, silt, and clay. The finer grained flood-plain, lacustrine, and marsh deposits underlie most of the study area.

Where present, fine-grained deposits would restrict vertical movement of ground water. However, past studies and available data indicate that the near-surface deposits consist of discontinuous silts and clays and that few intervening clay layers are between the fine-grained surficial deposits and the underlying E clay of Croft (1972). Miller and others (1971, p. 28) reported that near-surface deposits laid down in flood basins by the overflow of the San Joaquin and Kings Rivers consist largely of a discontinuous layer of impervious clay and clay adobe intermixed with river-channel deposits of sand and gravel. In contrast, the older and deeper flood-plain deposits are coarser and contain less clay.

Lithologic logs from auger holes previously drilled throughout the Kesterson National Wildlife Refuge by the U.S. Bureau of Reclamation and the California Department of Water Resources (U.S. Bureau of Reclamation, written commun., 1985) show that at numerous locations, alluvial deposits consist entirely of silty sand, however, at other locations, clayey and silty beds at land surface may be 20 feet or greater in thickness. Below the surficial flood-plain deposits, the older continental deposits consist predominately of coarse-textured sands with some silt and clay (U.S. Bureau of Reclamation, written commun., 1985). The only continuous clay layer found in this area is the E clay mapped by Croft (1972). Croft's E clay includes the Pleistocene Corcoran Clay Member of the Tulare Formation. It ranges in depth from 180 feet just east of the San Joaquin River to about 260 feet in the western part of the study area; and ranges in thickness from about 60 to 100 feet (R.W. Page, U.S. Geological Survey, written commun., 1985).

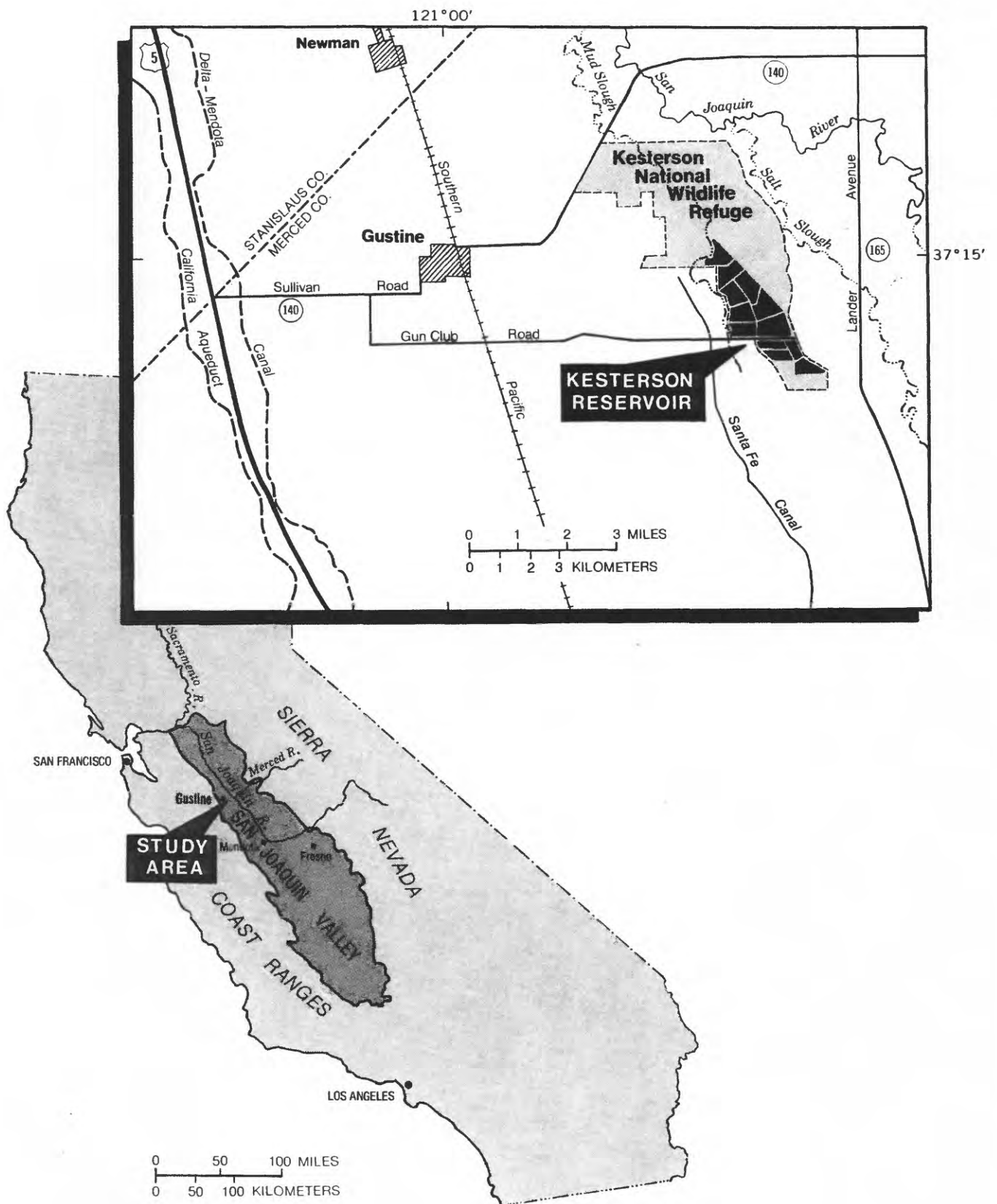


FIGURE 1. Location of study area.

## Ground-Water Hydrology

Ground water in the study area occurs in at least two distinct regional aquifers: an unconfined aquifer above the E clay (upper zone), and a confined aquifer below the E clay (lower zone) (Hotchkiss and Balding, 1971, figs. 10-12 and pl. 1; Davis and Poland, 1957, pl. 30; and Page, 1973). This study is concerned primarily with the upper-zone aquifer.

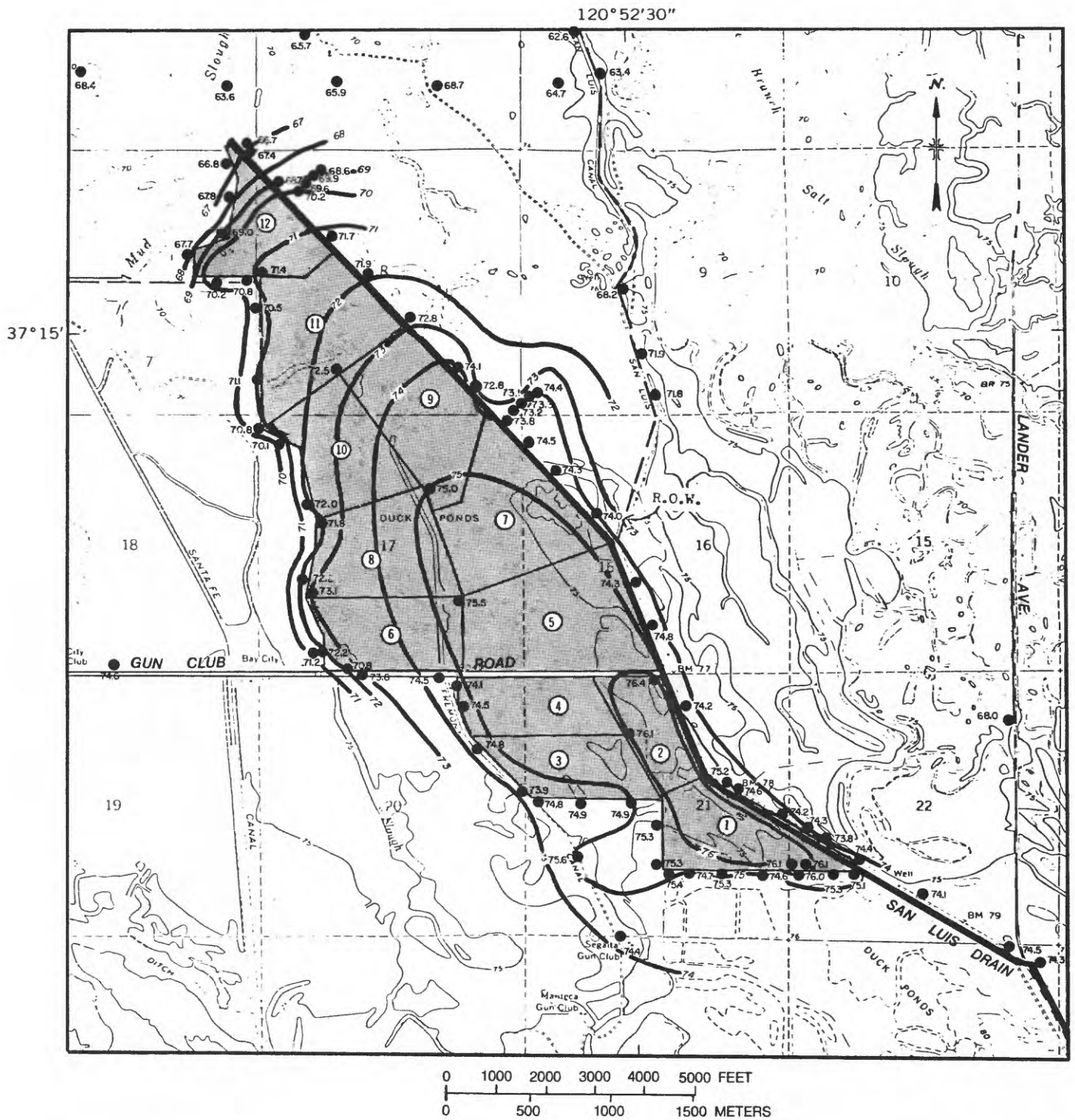
Under natural conditions, ground water moved northward and northeastward from the western foothills toward the valley trough and then northwest toward the delta area. Water recharged the aquifer system by seepage from west-side streams and infrequent flooding. Recharge from precipitation occurred during winter months. Where shallow silt and clay layers existed, the downward movement of ground water was restricted and a shallow semiperched aquifer was formed. Slow downward movement of ground water occurred in recharge areas where vertical head gradients were downward. Where the silt and clay lenses were absent, the upper-zone aquifer was recharged more rapidly. Near the valley trough, upward ground-water movement from the lower-zone aquifer through the underlying E clay to the upper-zone aquifer occurred (Williamson and others, 1985, and Hotchkiss and Balding, 1971, p. 46-47). Discharge from the aquifer system was by slow upward movement in the valley trough to surface waterways and by evapotranspiration during the summer months. The valley trough has historically had flowing wells and the water table has been very shallow (Mendenhall and others, 1916, pl. 1).

As the aquifer was increasingly stressed by pumping from the early 1900's to the mid-1960's, ground water continued to move in a northeastward and northward direction, but in places, pumping depressions that developed east of the trough caused ground water to move across the valley trough and into the depressions (Williamson and others, 1985). Extensive regional pumping of the lower-zone aquifer caused heads in this aquifer to be

lower than in the upper-zone and shallow aquifers. This has resulted in slow downward ground-water movement through the E clay. A generalized water-level-contour map of the lower-zone aquifer (Williamson and others, 1985) indicates that heads in that zone are lower than those in the upper-zone aquifer.

After the widespread application of irrigation water, ground-water recharge was predominately through irrigation return and seepage from canals and west-side streams. The seasonal flooding of duck ponds throughout the area results in increased recharge during the winter and spring months. Discharge from the aquifer is through upward and lateral movement of ground water to the sloughs in the area, evapotranspiration during the summer months, ground-water outflow toward the east to the San Joaquin River and north toward the delta area, and through downward movement of ground water into the underlying lower-zone aquifer.

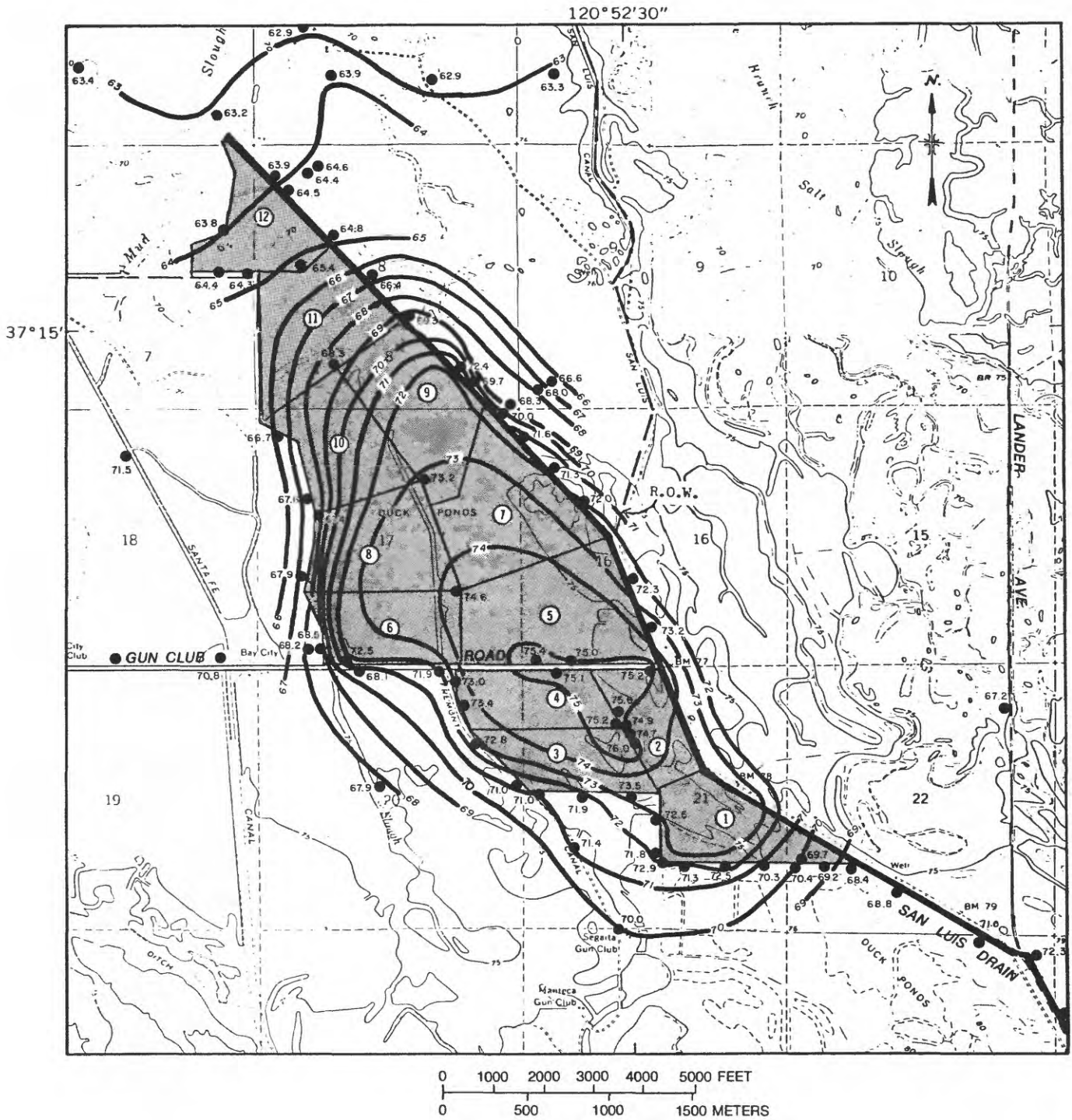
In the study area, wells generally less than 25 feet deep are used to measure water levels (L.E. Phillips, U.S. Bureau of Reclamation, oral commun., 1985). Water levels in these wells range in depth below land surface from about 2 to 25 feet, with most water levels within 15 feet of land surface. Water-level contour maps using these wells were prepared by the U.S. Bureau of Reclamation (L.E. Phillips, U.S. Bureau of Reclamation, written commun., 1985). Two of these maps (figs. 2 and 3) were prepared for January 1985 and August 1985. These maps show that under current conditions, ground-water levels decrease in all directions away from Kesterson Reservoir. This implies ground-water movement away from Kesterson Reservoir to the east and northeast toward Salt Slough, to the northwest, west, and southwest toward Mud Slough, and to the south. Ground-water movement is also to the northwest from pond 1 to pond 12, as implied by the decline in ground-water levels to the northwest. These general flow patterns are true for winter- and summer-flow conditions. The difference between these two times of the year is that regional



**EXPLANATION**

-  WATER-LEVEL CONTOUR - Shows altitude of water level. Contour interval 1 foot. Datum is sea level
-  WELL - Number is altitude of water level, in feet above sea level
-  KESTERSON POND NUMBER

FIGURE 2. Water-level contours for the shallow aquifer in the vicinity of Kesterson Reservoir, January 1985.



**EXPLANATION**

-  **WATER-LEVEL CONTOUR** - Shows altitude of water level. Contour interval 1 foot. Datum is sea level
-  **WELL** - Number is altitude of water level, in feet above sea level
-  **KESTERSON POND NUMBER**

FIGURE 3. Water-level contours for the shallow aquifer in the vicinity of Kesterson Reservoir, August 1985.

ground-water levels are higher during the winter (fig. 2) than during the summer (fig. 3) and the gradient away from Kesterson Reservoir is greater during summer than the winter.

This seasonal trend is evident in all of the hydrographs examined for the Kesterson area. Figure 4 shows a hydrograph of water levels measured in well 8S/10E-21L4M by the U.S. Bureau of Reclamation. The water levels fluctuate seasonally, with highest levels generally occurring during the late winter months and lower levels occurring during the late summer months. These seasonal fluctuations may be largely attributed to the cycle of flooding surrounding duck ponds in the early fall and draining them in the spring. Additional causes of water-

level declines from spring to fall may be by ground-water loss through evapotranspiration or any undocumented ground-water pumping in the area. As can be seen from figure 4, this seasonal trend has taken place for more than 30 years starting prior to the construction of the Kesterson Reservoir (1972) and has continued since then. Also evident is a long-term rise in water levels that might be attributed to the increase in regional application of surface water to land surface in the form of irrigation, seasonal flooding of duck ponds, drainage water stored in Kesterson Reservoir, or recovery from regional pumping. This rise in shallow water levels was measured previously in much of the trough area on the west side of the San Joaquin Valley (Hotchkiss and Balding, 1971).

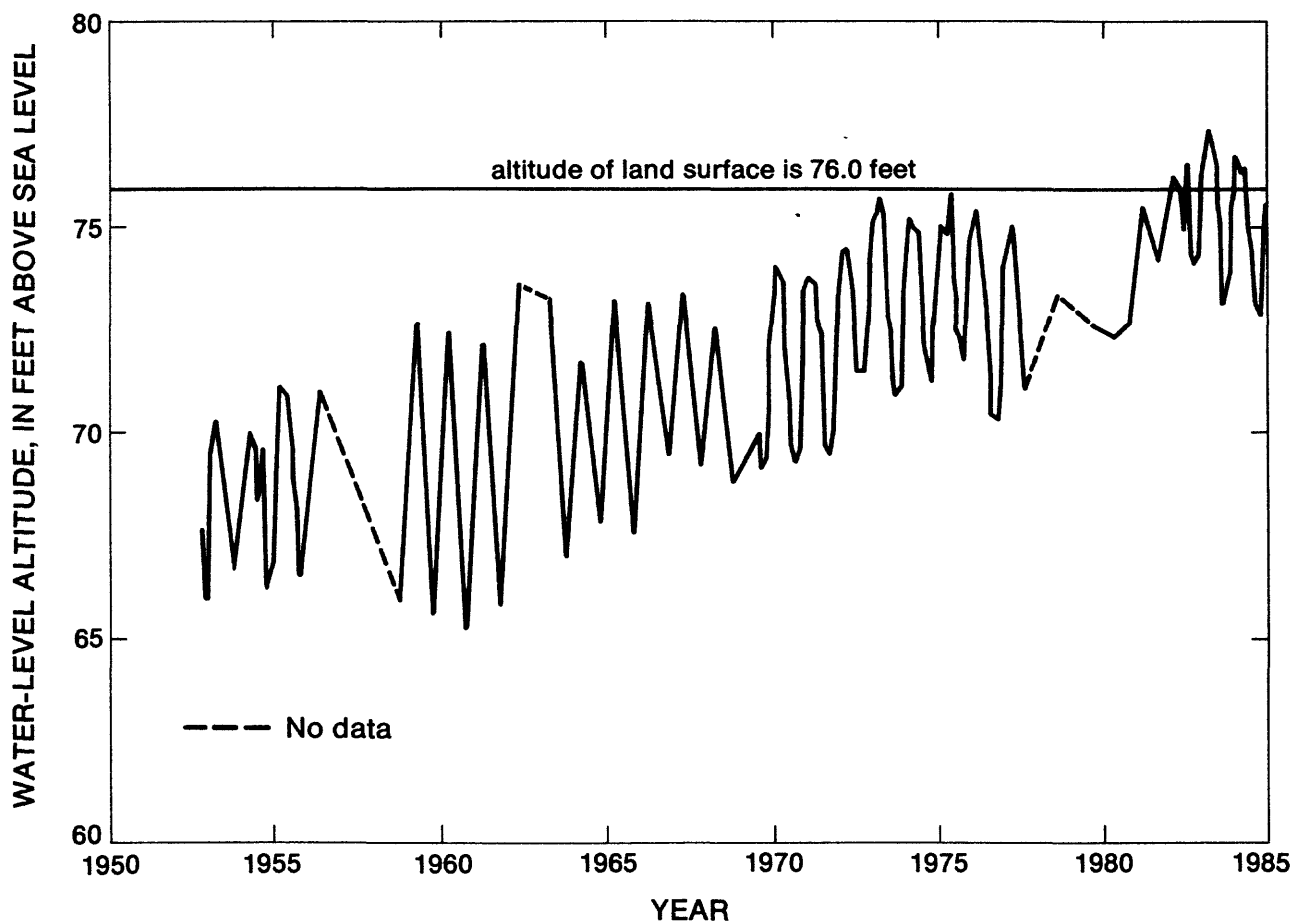


FIGURE 4. Water levels measured in well 8S/10E-21L4M, 1950-85.

## MODELING GROUND-WATER FLOW

A ground-water flow model is used to simulate the distribution of hydraulic head and volumetric flow rates in the modeled area. This is done by solving the ground-water flow equation, given estimates of hydraulic properties of porous materials, hydraulic stresses on the ground-water system, and initial and boundary conditions for the modeled area. Details concerning the model computer program may be found in McDonald and Harbaugh (1984).

### Governing Equation

The ground-water flow equation that is solved, is for three-dimensional ground-water flow of a homogeneous compressible fluid through a nonhomogeneous anisotropic aquifer. It is described by the following partial differential equation (McDonald and Harbaugh, 1984, p. 7):

$$\frac{\partial}{\partial x} \left( K_{xx} \frac{\partial h}{\partial x} \right) + \frac{\partial}{\partial y} \left( K_{yy} \frac{\partial h}{\partial y} \right) + \frac{\partial}{\partial z} \left( K_{zz} \frac{\partial h}{\partial z} \right) = S_s \frac{\partial h}{\partial t} + W \quad (1)$$

where

$K_{xx}$ ,  $K_{yy}$ ,  $K_{zz}$  are the hydraulic conductivity values along the principal coordinate axes of the hydraulic conductivity tensor (L/T),

$x, y, z$  are the cartesian coordinates aligned with the principal coordinate axes (L),

$h$  is the hydraulic head (L),

$S_s$  is the specific storage (1/L),

$t$  is time (T), and

$W$  is a source or sink term representing volumetric fluxes per unit volume (1/T).

This flow equation describes the flow of ground water and does not account for transport of solutes in the ground-water flow system.

### Boundary Conditions

Three types of boundary conditions may be used in this model, prescribed head (Dirichlet), prescribed flux (Neumann) or head dependent flow (Cauchy) boundaries. For a prescribed head boundary, a measured or estimated hydraulic head is assigned to boundaries where the hydraulic head in the aquifer does not change over time. At prescribed flux boundaries, an estimated flux is assigned. This value may represent flow into or out of the modeled area. Head-dependent sources or sinks are a flux boundary that is allowed to vary as a function of the head in the aquifer.

### Head Dependent Ground-Water Sources and Sinks

The rate of ground-water flow from sources or to sinks may be dependent on the difference between hydraulic head in the aquifer and some other datum such as the hydraulic head in a stream or drain, or depth below land surface altitude. These are referred to as head dependent ground-water sources or sinks and are used in the Kesterson model. A discussion of the functioning of these head-dependent ground-water sources and sinks is included to explain to the reader how water is added or extracted from the ground-water system and the general limitations of these methods.

The exchange of ground water between a surface-water body such as a river, canal, or pond, and the adjacent aquifer system is controlled by the difference in hydraulic head in the aquifer system and the hydraulic head in the surface-water body, and the conductance of the porous material between the two. The equation representing this exchange of ground water is (McDonald and Harbaugh, 1984, p. 209):

$$Q = \frac{K' LW}{M} (HRIV - HAQ) \quad (2)$$

where

- Q is volumetric flux between the surface-water body and the underlying aquifer (L/T),
- K' is vertical hydraulic conductivity of material at bottom of surface-water body (L/T),
- L is length of surface-water body (L),
- W is width of surface-water body (L),
- M is thickness of material at bottom of surface-water body (L),
- HRIV is hydraulic head in the surface-water body (L), and
- HAQ is hydraulic head in the underlying aquifer (L).

Figure 5 shows a conceptualization of the model representation of a duck pond or river. Figure 6 illustrates how this representation functions in the model. If the hydraulic head in the aquifer is above the hydraulic head in a surface-water body, water moves out of the aquifer at rates controlled by this head difference and bottom-material conductance. As the head in the aquifer declines, the flow rate decreases until the head in the aquifer equals the head in the surface-water body. At this point, there is no exchange of water. As the head in the aquifer declines below the hydraulic head in the surface-water body, water leaks into the aquifer. The rate of leakage increases until the

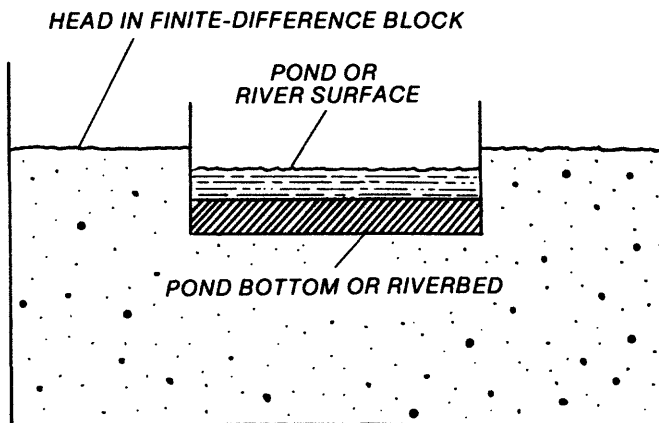


FIGURE 5. Model representation of a duck pond or river (adapted from McDonald and Harbaugh, 1984, fig. 34a).

hydraulic head in the aquifer declines below the altitude of the bottom of the surface-water body. The rate of leakage into the aquifer remains constant as long as the hydraulic head is less than the altitude of the bottom of the surface-water body. Water released from storage from the bottom materials of the surface-water body and hydraulic head change in the surface-water body due to inflow or outflow of water are not accounted for.

Another head-dependent ground-water sink function used in this model describes evapotranspiration losses. The evapotranspiration rate from an unconfined ground-water system may be dependent on depth of hydraulic head in the aquifer below land surface.

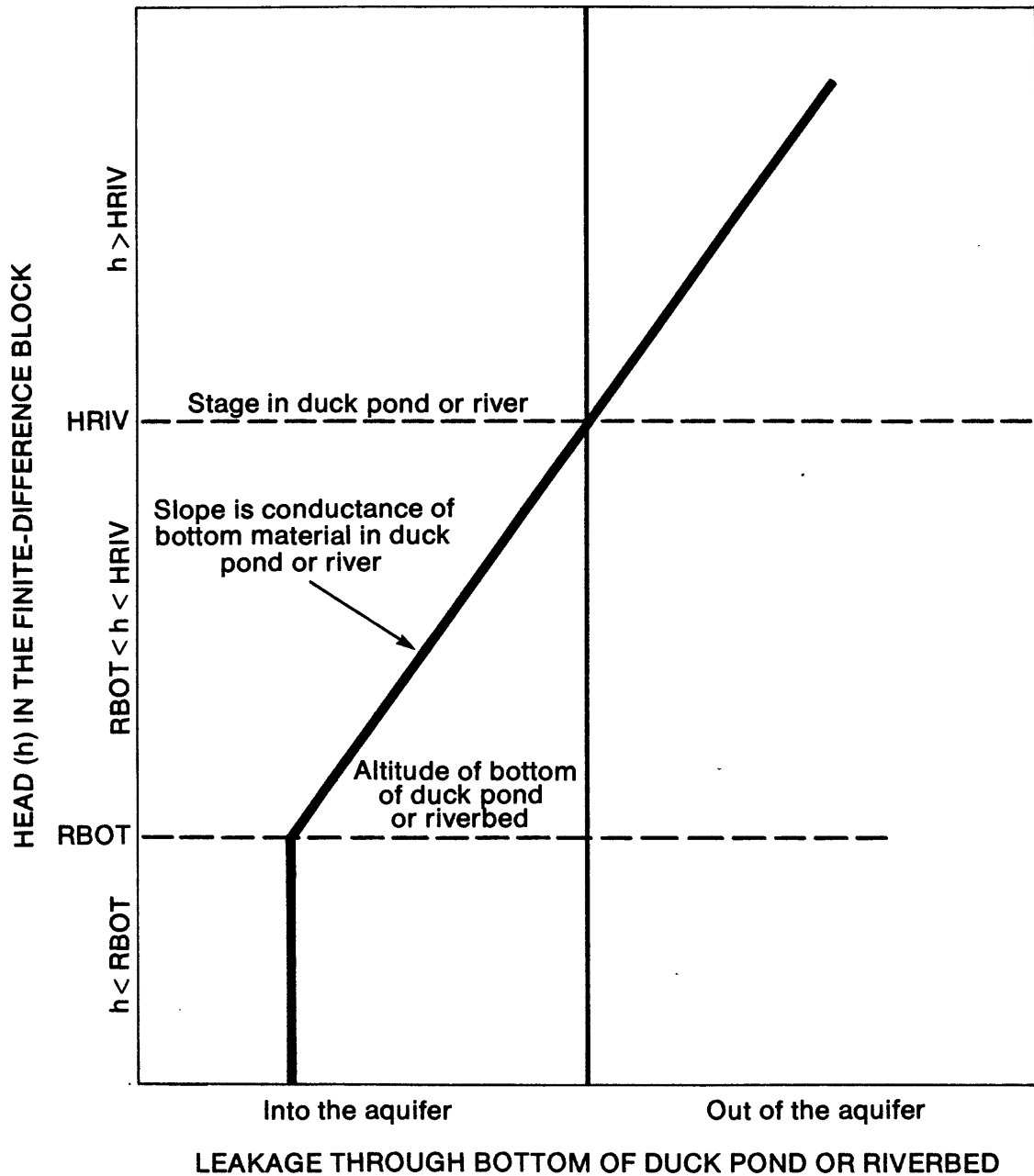
The equation describing evapotranspiration as a head-dependent function (from McDonald and Harbaugh, 1984, p. 318) is:

$$Q_{et} = ETRATE (H_a - (SURF-EXDP))/EXDP \quad (3)$$

where

- $Q_{et}$  is rate of evapotranspiration (L/T),
- $H_a$  is hydraulic head in the aquifer (L),
- ETRATE is maximum rate of evapotranspiration (L/T),
- SURF is elevation of evapotranspiration surface (L), and
- EXDP is depth below the evapotranspiration surface at which evapotranspiration ceases (L).

Figure 7 illustrates that when the hydraulic head in the aquifer is at or above the evapotranspiration (ET) surface, ground water is lost at the maximum ET rate. As the hydraulic head in the aquifer declines, the ET rate decreases until the critical ET depth (EXDP) is reached. When the head in the aquifer is at or below this depth, there is no evapotranspiration. The source of water lost through ET is the ground-water reservoir. The model does not extract evaporation from surface water and thereby decrease the water level in the surface-water body.



**EXPLANATION**

HRIV is head (stage) in the duck pond or river  
 RBOT is altitude of the bottom of duck pond or riverbed

FIGURE 6. Head dependent ground-water source or sink function (adapted from McDonald and Harbaugh, 1984, fig. 37).

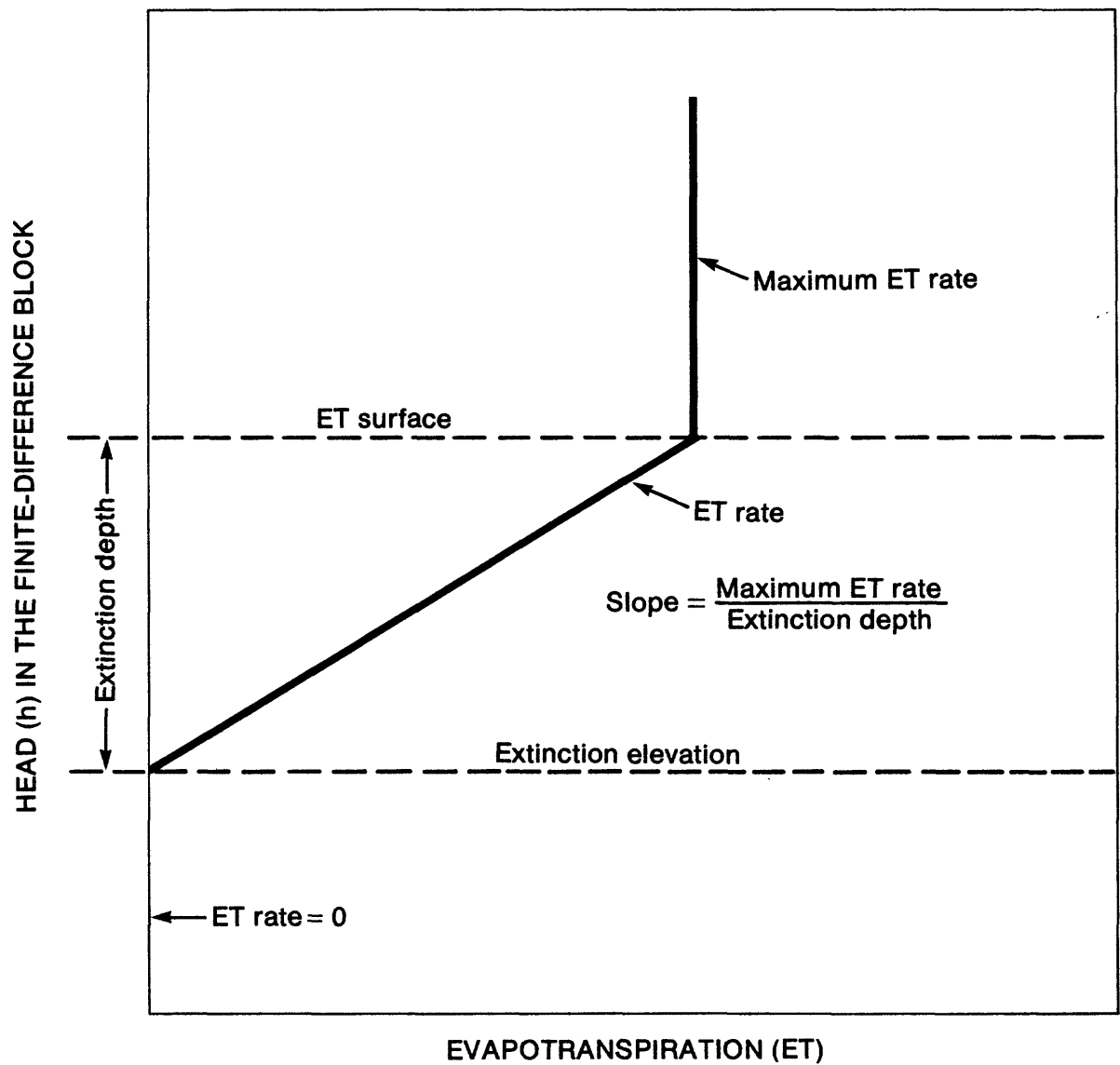


FIGURE 7. Evapotranspiration as a function of head in the aquifer (from McDonald and Harbaugh, 1984, fig. 42).

## Numerical Methods

In problems where aquifer geometry and hydraulic properties cannot be idealized, an exact solution to equation 1 cannot be found. An approximate solution can be obtained using numerical methods such as finite differences. The derivations of the finite-difference approximation to equation 1 is found in McDonald and Harbaugh (1984).

The slice-successive-over-relaxation (SSOR) method and the pre-conditioned conjugate gradient (PCG) method were used to solve the finite-difference equations numerically. The PCG method was used in certain transient simulations in which SSOR failed to converge. A description of the SSOR method is in McDonald and Harbaugh (1984, p. 432) and the PCG method is in Kuiper (1981).

## MODEL DESIGN AND DEVELOPMENT

### Finite-Difference Grid

The modeled area is shown in figure 8. The modeled area covers 124 square miles and includes more than just the area in the immediate vicinity of Kesterson Reservoir. This was done to include more of the regional ground-water flow system in the model.

The finite-difference grid used for this model (fig. 8) consisted of 78 rows by 67 columns, or 5,226 nodes per layer. A variable grid spacing was used so that a small grid spacing of 500 feet could be used in the Kesterson Reservoir area and increased to 4,000 feet in outlying areas where a high degree of detail was not required.

Three layers were used to represent the unconsolidated material above the E clay. The thickness of material above the E clay ranges from 180 feet to about 260 feet. An average thickness of 220 feet was used to represent an approximate total thickness of deposits above the E clay. One layer was used to represent about 20 feet of fine-grained unconsoli-

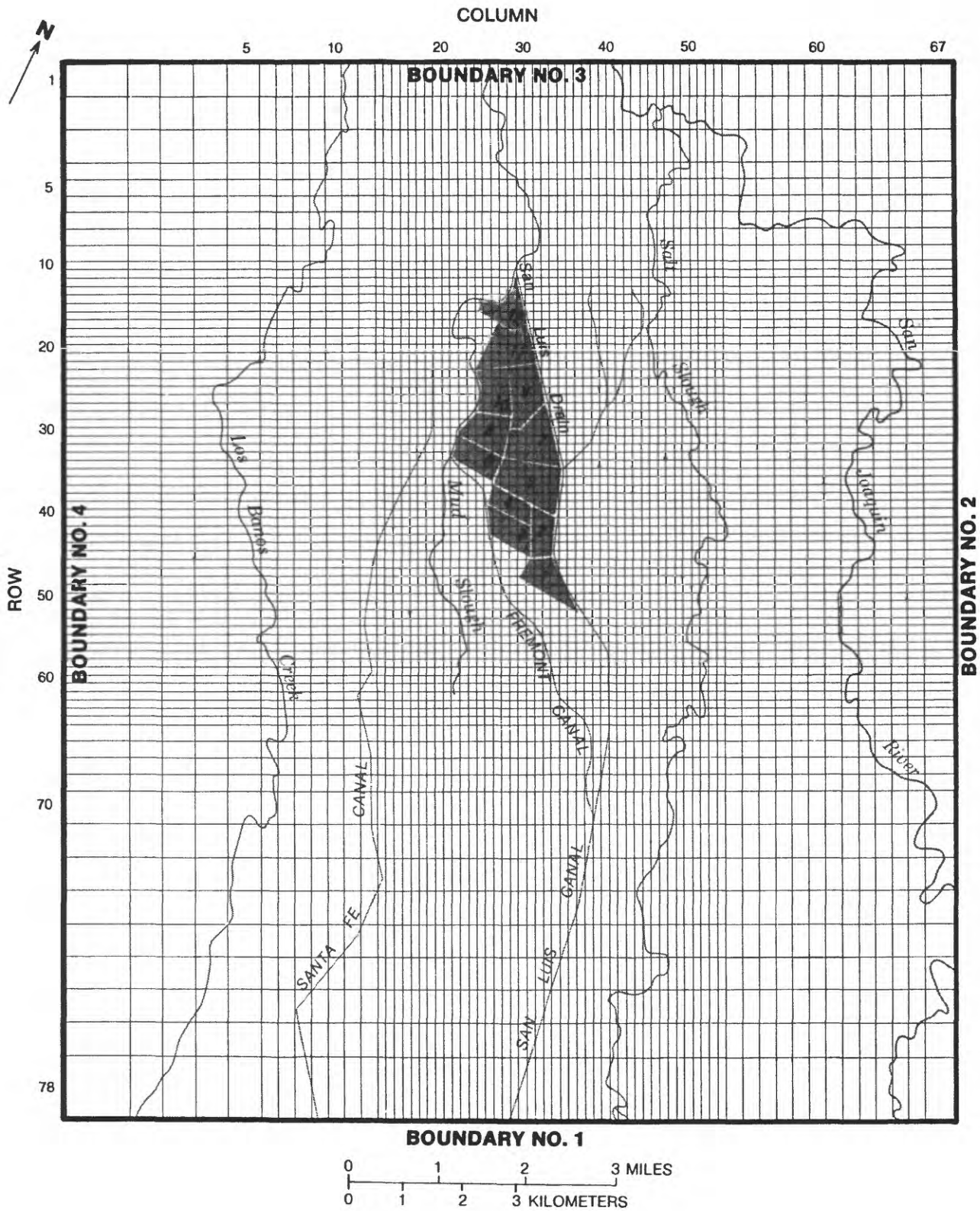
dated materials found at or near land surface. The 20-foot thickness is an approximation. Lacustrine and marsh deposits in this area may be greater than 20 feet in some instances, but may not exist in others. Each of the bottom two layers were 100 feet thick to represent the remaining coarser-grained material above the E clay.

### Estimation of Vertical Hydraulic Conductivity for Streambeds, Canals, and Pond Bottoms

Estimates of vertical hydraulic conductivity (Kv) for the canals, streambeds, and pond bottoms represented in the model were derived from infiltrometer tests done by the U.S. Bureau of Reclamation and the California Department of Water Resources. Other sources of estimates were from calibration results from two model studies in the San Joaquin Valley by the U.S. Geological Survey and seepage studies done at Kesterson Reservoir by the U.S. Bureau of Reclamation.

Fifty-six infiltrometer tests were made by the California Department of Water Resources. Nineteen 1-foot diameter infiltrometers were placed in existing small duck ponds in the study area. They were then filled with water from the pond so that a head differential of about 1 foot existed between water inside and outside. Several measurements usually were made during a period of 5 to 10 days. The remaining 37 infiltrometers were placed in areas not covered by duck ponds. Water for these infiltrometers was taken from Salt Slough. All water used in the infiltration studies was assumed not to appreciably affect soil permeability.

The 33 infiltration tests made by the U.S. Bureau Reclamation were done by their standard methods, as described in U.S. Department of the Interior (1978, p. 81-93). In this technique, a 42-inch diameter hole is excavated to the test zone. The test area is inside an 18-inch cylinder. Two piezometers and two calibrated tensiometers are used for



**EXPLANATION**

KESTERSON POND AND POND NUMBER

FIGURE 8. Finite-difference grid used in model.

checking water levels and the degree of saturation. A float apparatus is installed for maintaining a constant 6-inch head in the cylinder. Estimates of Kv from all infiltrometer tests ranged from  $1.3 \times 10^{-8}$  to  $1.4 \times 10^{-4}$  ft/s.

Another estimate of Kv was made by the U.S. Bureau of Reclamation (written commun., 1984) by determining seepage rates out of individual ponds at Kesterson Reservoir. Estimates of pond seepage were calculated by subtracting estimated net evaporation from measured changes in pond storage.

Changes in pond storage were estimated using preliminary area-capacity curves. Net evaporation was estimated by the U.S. Bureau of Reclamation to be 3 to 4.5 ft/yr based on pan-evaporation measurements at Kesterson. During 1982, the total seepage from Kesterson was estimated to be 4,200 acre-feet (U.S. Bureau of Reclamation, written commun., 1984). The total pond area is about 1,200 acres. The seepage rate was calculated to be  $1.1 \times 10^{-7}$  ft/s. More recent estimates (U.S. Bureau of Reclamation, written commun., 1985) indicate that seepage rates from Kesterson Reservoir may be  $1.4 \times 10^{-7}$  ft/s.

Estimates of Kv for river and slough bottom material were obtained from Page (1977) and Londquist (1981). These range from  $5.2 \times 10^{-6}$  to  $5.2 \times 10^{-4}$  ft/s and were derived from calibration of digital flow models on the east side of the San Joaquin Valley.

A range of Kv values including the results of the infiltrometer tests and the seepage studies at Kesterson Reservoir were used in the model for the fine-grained material in the top 20 feet of sediment. This included the bottoms of ponds at Kesterson Reservoir, unlined canals, and duck ponds. These range from  $1.3 \times 10^{-8}$  to  $1.4 \times 10^{-4}$  ft/s. The values of vertical hydraulic conductivity used for the river and slough bottom material were those derived from Page (1977) and Londquist (1981). All values for Kv used in the model are included in table 1.

TABLE 1.--Values of horizontal (Kh) and vertical (Kv) hydraulic conductivity used in model simulations

Model parameter	Hydraulic conductivity (ft/s)	
	Low	High
Kh for layer 1 .....	$5.8 \times 10^{-7}$	$1.8 \times 10^{-4}$
Kh for layer 2 .....	$1.2 \times 10^{-5}$	$9.9 \times 10^{-4}$
Kh for layer 3 .....	$1.2 \times 10^{-5}$	$9.9 \times 10^{-4}$
Kv/b between layers 1 and 2 ...	$4.6 \times 10^{-9}$	$9.6 \times 10^{-7}$
Kv/b between layers 2 and 3 ...	$1.2 \times 10^{-8}$	$9.9 \times 10^{-7}$
Kv for ponds and canals .....	$1.3 \times 10^{-8}$	$1.4 \times 10^{-4}$
Kv for rivers and sloughs .....	$5.2 \times 10^{-6}$	$5.2 \times 10^{-4}$

Estimation of Horizontal and Vertical Hydraulic Conductivity for Model Layers 1, 2, and 3

The estimates of horizontal hydraulic conductivity of the alluvial deposits were obtained from auger tests made within the model area and from calibration results of digital models developed for the San Joaquin Valley. Fifty-two auger tests were done in the vicinity of Kesterson Reservoir by the California Department of Water Resources (written commun., 1967). Because of the instability of the saturated soil material, some boreholes collapsed, making open borehole permeability tests difficult. In these cases, the permeability tests were done using 2-inch diameter well points pushed into the material in the bottom of the auger hole. As a result, the material measured in these tests represent an aggregate of material penetrated by the auger hole. The method of conducting the permeability test in the open auger hole consisted of pumping two or three bore-hole volumes of water out of the auger hole to remove the smearing on the bore-hole wall caused by the auger. After water levels had stabilized, the bore hole was pumped dry and the water-level recovery with time was measured.

Gravity or low pressure permeability tests were done in the 2-inch diameter piezometers installed in the auger holes. In this test, a known head or quantity of water is added to the static column of water in the well. The quantity of water added to keep water levels constant with time or the decline in water levels with time is recorded.

The values of  $K_h$  estimated from the auger tests ranged from  $5.8 \times 10^{-7}$  to  $1.8 \times 10^{-4}$  ft/s. Most of these tests were conducted in the top 20 feet of sediment with only a few tests measuring the hydraulic conductivity of the deeper material. From this limited data there does not seem to be a vertical trend to these estimates. Low and high values of  $K_h$  were in the shallow and deeper sediments. Low values of  $K_h$  were assigned to the finer grained surface material and higher values to the deeper material since it tends to be more coarse grained. This was based strictly on gross lithologic variations and not a statistical analysis of data. A single value of hydraulic conductivity was assigned to each aquifer layer because information was not available to identify spatial trends in  $K_h$  within any aquifer layer.

Hydraulic conductivity values ranging from  $5.8 \times 10^{-7}$  to  $1.8 \times 10^{-4}$  ft/s from the auger tests were used for aquifer layer 1, and  $1.2 \times 10^{-5}$  to  $9.9 \times 10^{-4}$  ft/s, from the auger tests and digital models (Londquist, 1981 and Williamson and others, 1985) were used for aquifer layers 2 and 3. The vertical hydraulic conductivity for each model layer in the model was assumed to be one-tenth the horizontal hydraulic conductivity used for that simulation. Data were not available to describe the ratio of vertical to horizontal hydraulic conductivity. This anisotropy ratio was based on the lithologic description of the unconsolidated deposits. These deposits consist predominately of sand with some salt and very few clay zones.

#### Estimation of Vertical Hydraulic Conductivity for E clay

Estimates of  $K_v$  for the E clay were obtained from Page (1977). A value of  $1.1 \times 10^{-10}$  ft/s was used in the preliminary model for Modesto, California (Page, 1977). Other estimates of  $K_v$  for the E clay were obtained from consolidation tests on cores from well KR-205A. These values were  $2.2 \times 10^{-10}$  and  $6.6 \times 10^{-11}$  ft/s. The value of vertical hydraulic conductivity from Page (1977) was used in estimating the vertical flux across the E clay from the lower-zone aquifer to the upper-zone aquifer.

#### Estimation of Specific Yield

Estimates of specific yield are needed for simulations in which the hydraulic head in the aquifers varies with time. Estimates for specific yield from aquifer tests are not available in the study area. Specific yield is generally 0.01 to 0.30 (Freeze and Cherry, 1979). Londquist (1981) and Page (1977) used a specific yield of 0.07 to 0.17. Specific yield estimates used in the Central Valley model (Williamson and others, 1985) ranged from 0.10 to 0.15. Initial estimates used in the Kesterson model are 0.10 for all aquifer layers, and were not varied during subsequent simulations.

#### Boundary Conditions

Prescribed flux boundaries were used around the entire perimeter of the modeled area (fig. 8). Boundary fluxes were estimated from water-level maps prepared by the California Department of Water Resources for the years 1981 through 1983. Head gradients across model boundaries were estimated from these maps, assuming the same horizontal head gradient for each model layer. These head gradients, together with estimates of hydraulic conductivity and cross-sectional area of the model boundaries

were used to calculate ground-water flow rate across the model boundaries using the following equation:

$$Q_{\ell} = \sum_{n=1}^3 (K_n A_n) \frac{dH}{dL} \quad \ell = 1,2,3,4 \quad (4)$$

where

$Q_{\ell}$  is flow rate across  $\ell$ th model boundary ( $L^3/T$ ),

$A_n$  is cross-sectional area of the  $n$ th model layer ( $L^2$ ),

$K_n$  is initial estimate of hydraulic conductivity for aquifer layer  $n$  ( $L/T$ ), and

$\frac{dH}{dL}$  is head gradient across  $\ell$ th model boundary (dimensionless).

Estimates of seasonal ground-water flow across model boundaries were calculated. These estimates varied slightly from year to year and from season to season. Flow-rate estimates were slightly greater for fall than for spring. Average flow rates (shown in table 2) were calculated for 1981-83 because flow differences between seasons were small and not consistent along all boundaries.

TABLE 2.--Average ground-water flow rates for each model boundary

Boundary No.	Flow rate (ft <sup>3</sup> /s)
1	0.18
2	.39
3	-.08
4	.92

The top of the E clay makes up the bottom boundary of the model. This clay is not impermeable but has a relatively low vertical hydraulic conductivity. The magnitude of flow rates across this clay will be controlled primarily by this low vertical hydraulic conductivity. The direction of flow will depend on the relative head differences above and below

the E clay. In the study area, four sites at which wells were completed were above and below the E clay. These were well numbers 8S/10E-6R23M, -6R22M, -5P21M, -5P20M; KR-203A-B and KR-205A-B. Of these, only wells 8S/10E-6R23M, -6R22M, -5P21M, and -5P20M were measured at the time of this study. Head data from these four wells show that the head gradient across the E clay is from above the clay to below the clay, indicating downward flow. The vertical head difference ranged from 0.6 to 10.4. Hydraulic-head measurements from these wells are listed in table 3. These data show a seasonal trend in the head gradient across the E clay. The minimum value was in April and the maximum in July. There may be a recovery in hydraulic head below the E clay during winter months so that the head gradients reverse and ground-water flow is upward through the E clay. Water levels had not been measured in the wells for the winter months at the time of this study.

TABLE 3.--Measured hydraulic heads in piezometers above and below E clay

Location No. ... USBR No. .... Depth (feet) ...	Above E clay (feet)	Below E Clay (feet)	Difference (feet)
	8S/10E-6R23M KR-201B	8S/10E-6R22M KR-201A	
	206.5	324.3	
4-30-85 .....	67.4	66.8	0.6
5-29-85 .....	65.5	60.2	4.3
6-25-85 .....	64.6	57.4	7.2
7-31-85 .....	64.0	53.6	10.4

TABLE 3.--Measured hydraulic heads in piezometers above and below E clay--Continued

Location No. ... USBR No. .... Depth (feet) ...	Above E clay (feet)	Below E Clay (feet)	Difference (feet)
	8S/10E-5P21M KR-202B	8S/10E-5P20M KR-202A	
	216.0	324.7	
4-30-85 .....	--	66.0	--
5-29-85 .....	--	60.7	--
6-25-85 .....	66.3	58.5	7.8
7-31-85 .....	65.4	55.4	10.0

The flux across the E clay for each node in the bottom model layer was calculated by:

$$Q_{i,j,3} = K_v * A_{i,j} * \frac{\Delta H}{\Delta L} \quad (5)$$

where

$Q_{i,j,3}$  is flow rate assigned to node  $i,j$ , in layer 3 representing flow across the E clay ( $L^3/T$ ),

$K_v$  is estimated vertical hydraulic conductivity of the E clay ( $L/T$ ),

$A_{i,j}$  is surface area of finite-difference block  $i,j$  ( $L^2$ ), and

$\frac{\Delta H}{\Delta L}$  is hydraulic head gradient across E clay (dimensionless).

An estimated vertical hydraulic conductivity of  $1.1 \times 10^{-10}$  ft/s, a total surface area of  $3.5 \times 10^{+9}$  ft<sup>2</sup> (124 mi<sup>2</sup>), an average vertical head difference of 5.62 feet (wells KR-201B and KR-201A), and a distance between measuring points of 118 feet yields a total flow across the E clay of 0.02 ft<sup>3</sup>/s. This represents flow out of the upper-zone aquifer.

### Head Dependent Ground-Water Sources and Sinks

#### Rivers, Sloughs, and Canals

The San Joaquin River, Mud and Salt Sloughs, Los Banos Creek, Santa Fe, Fremont, and San Luis Canals cross the study area. Streamflow and stage-altitude data are not available to detail seasonal flow in any of these surface waterways. In the San Joaquin Valley, seasonal surface-water flow characteristics are such that flows and stages are probably highest during the winter and spring months and lowest during the summer and fall months. These surface-water features were modeled as head-dependent sources or sinks that are present during the entire year. The part of the San Luis Canal that delivers water to Kesterson Wildlife Refuge during the winter months is dry during

the summer months, so that it is not included in simulations covering that time of year. Since few of the data needed to simulate these surface-water bodies as head-dependent functions are available, these data had to be estimated. These data are the stage of the water body at different locations, the altitude of stage above the channel bottom, the vertical hydraulic conductivity of the channel-bottom material, and the surface area of the channel contained in each finite-difference block.

The stage altitude and the surface area of each of the rivers and canals were estimated from 7.5-minute topographic maps and from the results of elevation surveys done for the U.S. Bureau of Reclamation. Errors in these stage-altitude estimates are probably within 3 to 4 feet of actual stage altitudes. The elevation of water levels in the channels above channel bottoms was assumed to average 4 feet. The stage altitude, channel area, and channel depth estimates did not change from initial estimates during subsequent simulations. Seasonal stage fluctuations undoubtedly occur, but because they were unknown, stages in these surface-water bodies were assumed to remain constant with time. The vertical hydraulic conductivity estimates for the canals were assumed to be the same as results of the infiltrometer tests and those estimated from seepage studies at Kesterson Reservoir (table 1). The values of vertical hydraulic conductivity used for bottom material in the San Joaquin River, Los Banos Creek, and Salt and Mud Sloughs were taken from model studies in the San Joaquin Valley (Page, 1977 and Londquist, 1981).

Estimates of channel-bottom conductance are needed for each finite-difference block containing a river or canal in the model. These were calculated by multiplying vertical hydraulic conductivity by the channel area in each finite-difference block and dividing by the channel-bottom thickness, which was assumed to be 1 foot.

## Duck Ponds

Duck ponds cover about 18 percent of the land surface in the study area during the winter months. These ponds are flooded areas that are low lying or have earth embankments to hold in water. These ponds are filled with imported water in early fall and drained some time in the spring, after duck-hunting season. The source of this water is from irrigation canals and agricultural drainage.

Duck ponds were modeled as head-dependent sources or sinks that are present only part of the year. The direction of ground-water flow depends on the head difference between water levels in the duck ponds and the hydraulic head in the underlying aquifer. The rate of flow is largely dependent on the vertical hydraulic conductivity of the material making up the bottom of the duck ponds. The water levels of the duck ponds were unknown for the 124 mi<sup>2</sup> surrounding Kesterson Reservoir. Using 7.5-minute topographic maps, altitude surveys done for the U.S. Bureau of Reclamation, and aerial photographs, the average altitude of land surface and areal extent of each duck pond were estimated. There was some uncertainty in determining whether all flooded areas should be explicitly simulated in the model. Certain low-lying areas flood during the winter and spring months because of ground-water seepage or overland runoff. These areas, covering about 10 percent of the land surface in the study area, were not simulated using head-dependent source or sink functions. Instead, these areas remained active and simulated hydraulic heads were allowed to rise above land surface.

Each duck pond, when full, was assumed to contain an average of 1.5 feet of water. The water level in each duck pond was then estimated by adding 1.5 feet to the average land-surface altitude for each pond. The vertical hydraulic conductivity for the bottom material of the ponds were taken from table 1. The vertical hydraulic conductance was calculated by multiplying vertical hydraulic

conductivity by the area of the finite-difference block covered by the duck pond and dividing by the thickness of the bottom material. This thickness was assumed to be 1 foot.

## Kesterson Reservoir

Kesterson Reservoir is made up of 12 evaporation ponds that are operated throughout the year. On the average, stage measurements made in each pond since 1982 show that highest water levels are generally during the winter and spring months (U.S. Bureau of Reclamation, written commun, 1984). This is the same time of year that duck ponds covering large areas surrounding Kesterson are flooded to attract migratory waterfowl. After the migratory season is over, the flooded areas are drained and the land is used for pasture during the summer months. Water levels in the reservoirs generally decline and in some instances the reservoirs were reported to be dry.

The ponds at Kesterson were modeled as head-dependent sources that are in operation during the entire year. As with the rivers, canals, and duck ponds, the quantity of ground-water recharge is dependent on the difference between water levels in the reservoirs and hydraulic head in the underlying aquifer. Ground-water flow rates are largely controlled by the vertical hydraulic conductivity of the bottom material of the reservoirs. The water levels in reservoirs were obtained from weekly measurements made by the U.S. Bureau of Reclamation since 1982. The water-level measurements used for each pond were averaged for November through April and May through October, representing average winter-spring and summer-fall conditions. Average water levels used for the winter-spring conditions are higher than those used for summer-fall conditions for the same pond. These average pond levels are listed in table 4. Water levels in both cases are higher than water levels in surrounding duck ponds (winter only) or land-surface elevation.

TABLE 4.-- Average water levels in Kesterson Reservoir ponds used for winter-spring and summer-fall flow simulations

Pond No.	Average water levels (ft)	
	Winter-spring	Summer-fall
1	77.3	76.6
2	77.4	76.7
3	76.8	75.5
4	76.4	75.5
5	76.0	75.1
6	76.0	74.5
7	75.2	73.7
8	75.5	73.8
9	74.5	73.0
10	74.9	72.6
11	72.9	71.2
12	72.9	71.2

#### Evapotranspiration

Estimates of potential evapotranspiration from grass or pasture in the Central Valley are 52.5 in/yr (California Department of Water Resources, written commun., 1967). Based on average monthly evaporation data, about 77 percent of annual evapotranspiration occurs between mid-April through mid-October. This amounts to 40.3 inches during a 6-month period or  $2.1 \times 10^{-7}$  ft/s. The total evaporation for mid-October through mid-April is about 12.2 inches. Precipitation (10 to 15 inches) occurs during this time period. Precipitation approximately balances evaporation so that loss of water through evapotranspiration does not occur during this time period.

Data needed to simulate evapotranspiration are evapotranspiration rate, land-surface altitude, and an extinction depth below land surface at which ground-water loss through evapotranspiration ceases. The evapotranspiration rate was determined as described above. Land-surface

altitude was estimated from 7.5-minute topographic maps. The extinction depth was assumed to be 10 feet below land surface, based on ground-water studies in progress in southern California (W.R. Danskin, U.S. Geological Survey, oral commun., 1985). Evapotranspiration was extracted only from non-ponded areas.

#### MODEL SIMULATIONS

Two time periods and two types of model simulations were used to investigate the probable seasonal change in ground-water flow conditions. The first set of simulations was assumed to be steady-state winter-spring conditions for the purpose of assessing average ground-water flow conditions during the winter-spring season. The second set of simulations was of transient conditions during a 3-year period (April 1982 to March 1985) for the purpose of assessing the seasonal response of the aquifer system to the changing water levels in Kesterson Reservoir, to the draining and flooding of duck ponds surrounding Kesterson, and to ground-water losses through evapotranspiration. This 3-year period is a time period during which Kesterson Reservoir was receiving agricultural drainage water.

Because of uncertainty in estimates of horizontal and vertical hydraulic conductivity, and ground-water recharge and discharge rates, two model simulations were made to approximate a range of probable ground-water flow rates for the steady-state winter-spring, and 3-year transient simulations. The first simulation used the lowest estimates of horizontal hydraulic conductivities (table 1) for each aquifer layer and vertical hydraulic conductivity for the bottom materials at Kesterson Reservoir, duck ponds, rivers, sloughs, and canals. The second simulation used the highest estimates of horizontal and vertical hydraulic conductivity (table 1). The estimates of Kh for aquifers and Kv for fine-grained surface materials used in the model are shown in table 1.

## Simulation of Steady-State Winter-Spring Flow Conditions

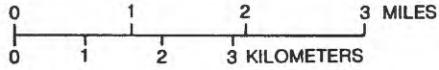
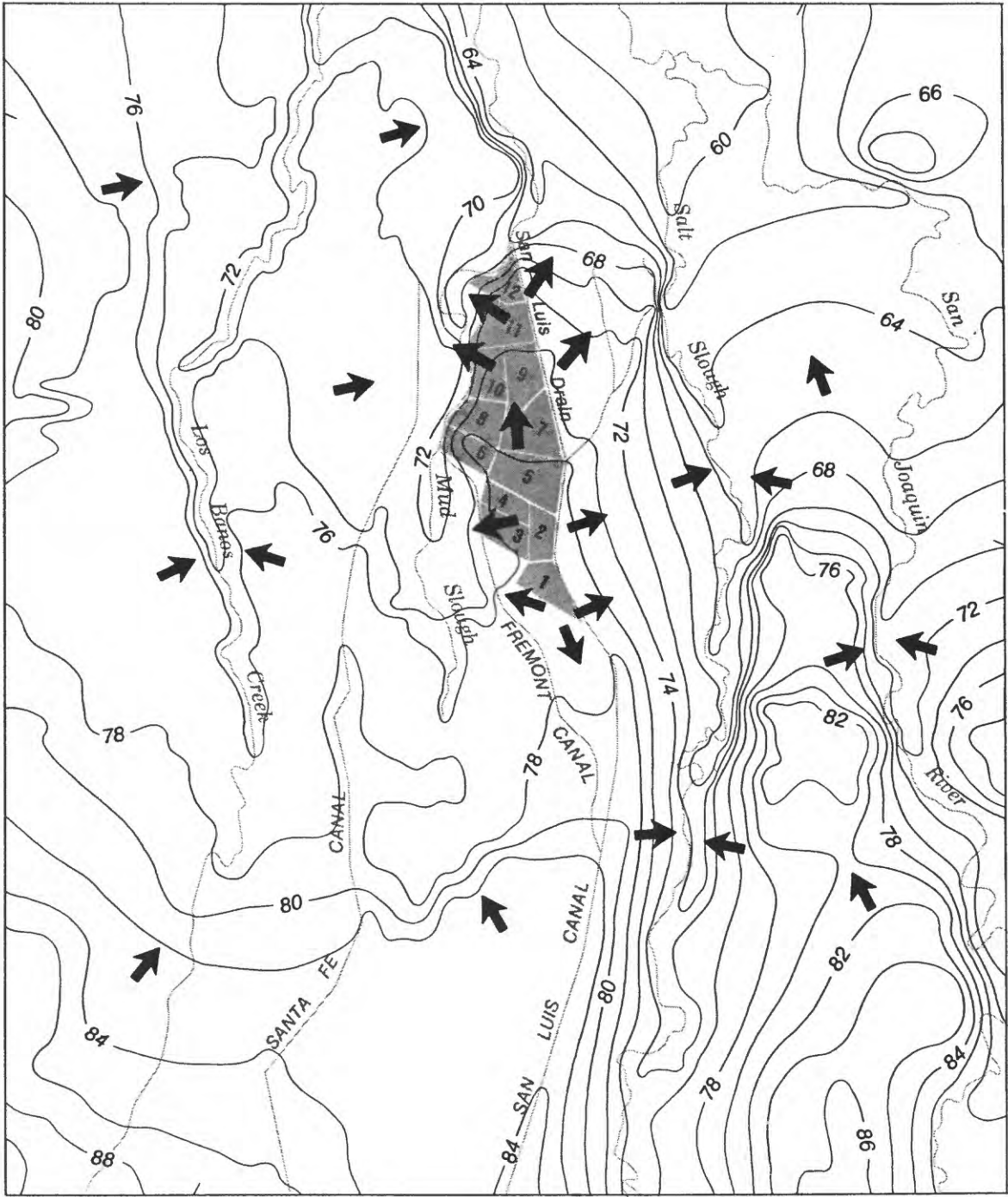
The winter-spring simulation included about 6 months during which the duck ponds are flooded and water levels in Kesterson Reservoir and ground-water levels are generally at their highest level. Long-term average winter-spring flow conditions are assumed to represent steady-state conditions. These winter-spring flow conditions were simulated using the higher stage altitudes in Kesterson Reservoir, flooded duck ponds, no evapotranspiration, and zero specific yield. During any year, there are no periods during which water levels are not changing, so that actual steady-state conditions are not reached. But, average winter ground-water flow conditions probably approach steady-state because the vast quantity of imported water flooding the duck ponds cause ground-water levels to rise to near land surface. In low-lying areas, water levels are actually above land surface. Additional rises in ground-water levels with time would be small even if the duck ponds remained filled for longer periods of time. The difference in hydraulic head between simulated winter steady-state conditions and average winter field conditions should then be small.

The results of the winter-spring simulations are shown as maps of hydraulic head for model layer 1 (figs. 9 and 10). The simulated hydraulic head distribution for the lower model layers is similar although somewhat smoother than the hydraulic-head distribution for model layer 1. For this reason, they are not shown. The direction of ground-water movement can be inferred from hydraulic-head gradients. Ground water moves from areas of high hydraulic head to areas where the hydraulic head is lower. Simulated hydraulic heads and inferred ground-water flow directions for the low and high values of hydraulic conductivities are generally similar. The major differences are in the top model layer (figs. 9 and 10).

Generally, the simulated hydraulic heads decrease from south to north (figs. 9 and 10). Regional ground-water flow directions are from the south and west toward the north and east to the San Joaquin River. In the study area, ground-water movement is from local recharge areas, such as Kesterson Reservoir, duck ponds and canals to local discharge areas such as Mud and Salt Sloughs, Los Banos Creek, and the San Joaquin River.

Ground-water flow, as inferred from the simulated hydraulic heads, is away from the Kesterson Reservoir in all directions (figs. 9 and 10). East of Kesterson Reservoir, the head gradient is away from Kesterson Reservoir to the east-northeast where it seems that ground-water flow is intercepted by Salt Slough. To the south, ground water seems to be flowing in a northerly direction. These simulations show ground-water flow from pond 1 to the south (figs. 9 and 10). All along the western border of Kesterson Reservoir, the simulated direction of flow is toward Mud Slough. The simulated hydraulic-head gradients are relatively steep in this area. Ground-water flow rates are greatest here as a result. These simulations do not show any ground-water flow from Kesterson that moves beyond Mud or Salt Sloughs. Ground water flows in a northerly direction beneath Kesterson Reservoir. This is due primarily to the water-level gradient in the Kesterson Reservoir ponds which decrease from south to north. North of Kesterson Reservoir, ground-water flow directions are to the northwest toward Mud Slough and north toward the San Joaquin River. These flow directions are consistent with hydraulic-head data measured around Kesterson Reservoir (fig. 2).

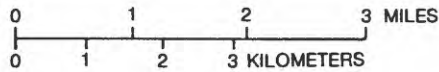
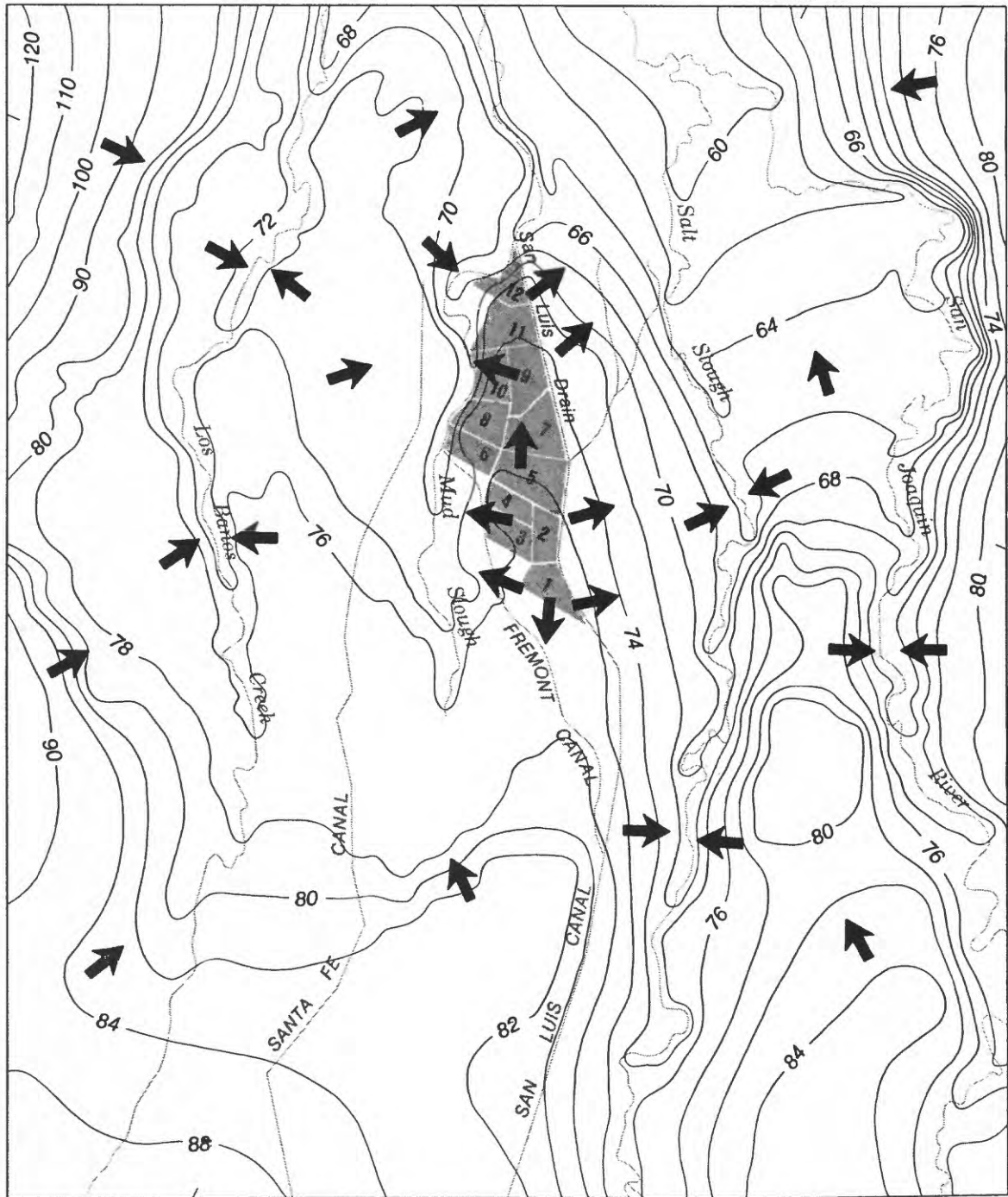
Vertical directions of ground-water flow between water bodies at land surface and the underlying aquifer and between model layers also were simulated. Simulated vertical ground-water flow is generally downward from Kesterson Reservoir and the duck ponds and canals to the underlying aquifer. Simulated directions of vertical ground-water flow beneath Mud Slough, Salt Slough, San Joaquin River,



**EXPLANATION**

-  SIMULATED DIRECTION OF GROUND-WATER MOVEMENT (NOT TO SCALE)
-  LINE OF EQUAL SIMULATED HYDRAULIC HEAD, IN FEET - Interval is variable
-  KESTERSON POND AND POND NUMBER

FIGURE 9. Hydraulic heads in model layer 1 for winter-spring flow conditions using high values of hydraulic conductivity.



**EXPLANATION**

-  SIMULATED DIRECTION OF GROUND-WATER MOVEMENT (NOT TO SCALE)
-  LINE OF EQUAL SIMULATED HYDRAULIC HEAD, IN FEET - Interval is variable
-  KESTERSON POND AND POND NUMBER

FIGURE 10. Hydraulic heads in model layer 1 for winter-spring flow conditions using low values of hydraulic conductivity.

and Los Banos Creek are upward from the underlying aquifer. Ground-water flow is also upward to low-lying areas that were not simulated as duck ponds and to certain duck ponds whose stage was lower than that of surrounding surface-water bodies. Using the higher values of vertical hydraulic conductivity for the bottom materials in the San Joaquin River, Mud Slough, Salt Slough and canals, these surface-water bodies exert a dominant effect on simulated hydraulic heads and on vertical ground-water flow rates. Using the lower values of hydraulic conductivity, simulated vertical ground-water flow is less because of the lower values of vertical hydraulic conductivity.

Comparison between simulated hydraulic heads for winter-spring flow conditions and measured winter-spring hydraulic heads is an indication of how well the model simulates average winter-spring flow conditions. Measured hydraulic heads were averaged for the winter and spring

months for May 1982 to March 1985. These comparisons are shown in table 5. The location of wells where water-level measurements were made are in figure 11.

Simulated hydraulic heads are generally distributed evenly above and below the average measured heads. The maximum difference between simulated and average measured heads is about 6 feet for both simulations. The average absolute value of the difference between simulated and average measured heads is 1.5 feet for the lower values of hydraulic conductivity and 1.6 feet for the higher values of hydraulic conductivity. There does not seem to be a spatial explanation for simulated heads above and below the average measured heads. All observation wells are located near surface-water bodies. If the stage altitude used to simulate these surface-water bodies are too high or too low, the simulated heads will also be either too high or too low. Estimated water budgets were not available to compare with simulated flow volumes.

TABLE 5.-- Comparison of simulated winter-spring hydraulic heads with measured hydraulic heads averaged for winter and spring months, May 1982 to March 1985

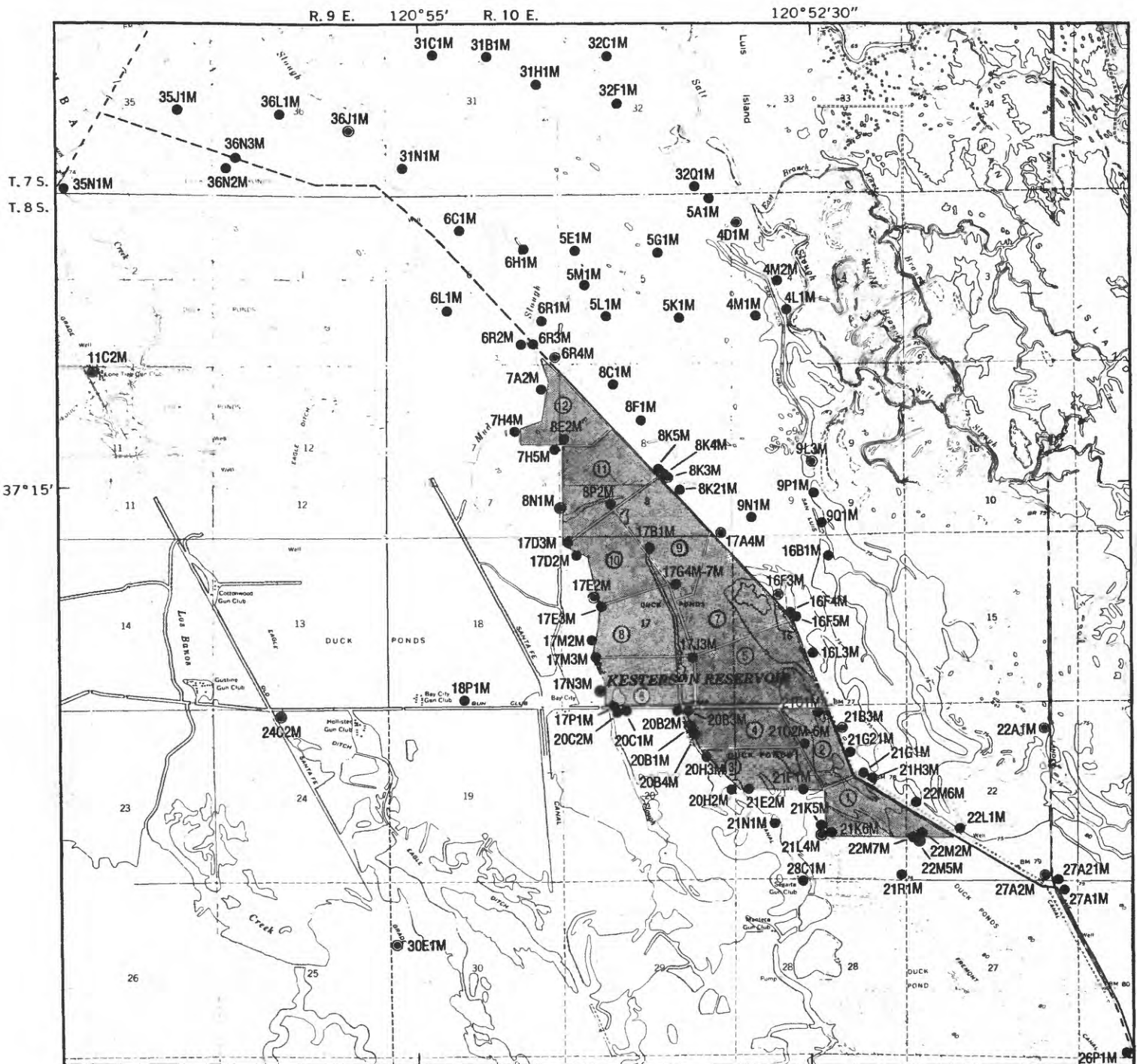
Location No.	USBR No.	Hydraulic heads			Difference between columns		
		Average measured (1)	Simulated using low K (2)	Simulated using high K (3)	1 and 2	1 and 3	2 and 3
7S/9E-35J1M	AP-198	68.2	67.6	69.0	0.6	-0.8	-1.4
-35N1M	G-11	68.1	65.0	65.1	3.1	3.0	-0.1
-36J1M	ER-81M	66.0	65.3	65.5	0.7	0.5	-0.2
-36L1M	ID-513	66.4	67.2	68.4	-0.8	-2.0	-1.2
-36N2M	AP-205	68.8	70.2	70.9	-1.4	-2.1	-0.7
-36N3M	DH-754	67.2	69.9	70.8	-2.7	-3.6	-0.9
7S/10E-31B1M	AP-325	61.5	61.0	60.9	0.5	0.6	0.1
-31C1M	AP-324	62.1	61.9	61.8	0.2	0.3	0.1
-31H1M	AP-307	62.5	61.2	61.1	1.3	1.4	0.1
-31N1M	AP-300	57.9	64.2	63.7	-6.3	-5.8	0.5
-32C1M	32C1	63.6	60.1	60.0	3.5	3.6	0.1
-32F1M	G-14	61.9	61.1	61.2	0.8	0.7	-0.1
-32Q1M	ER-76G	67.1	61.6	62.0	5.5	5.1	-0.4
8S/9E-11C2M	SF-2	68.5	72.9	73.9	-4.4	-5.4	-1.0
-24C2M	SF-6A	74.2	74.9	75.5	-0.7	-1.3	-0.6
8S/10E-4D1M	4D1	65.8	62.0	63.2	3.8	2.6	-1.2
-4L1M	AP-249	67.5	63.1	64.7	4.4	2.8	-1.6
-4M1M	AP-277	66.2	64.6	68.8	1.6	-2.6	-4.2

TABLE 5.-- Comparison of simulated winter-spring hydraulic heads with measured hydraulic heads averaged for winter and spring months, May 1982 to March 1985--Continued

Location No.	USBR No.	Hydraulic heads			Difference between columns		
		Average measured	Simulated using low K	Simulated using high K	1 and 2	1 and 3	2 and 3
		(1)	(2)	(3)			
8S/10E-4M2M	AP-407	66.6	63.1	68.4	3.5	-1.8	-5.3
-5A1M	AP-247	67.1	62.0	62.8	5.1	4.3	-0.8
-5E1M	AP-284	65.9	64.9	65.2	1.0	0.7	-0.3
-5G1M	AP-285	65.2	64.1	65.7	1.1	-0.5	-1.6
-5K1M	AP-346	67.0	66.2	69.1	0.8	-2.1	-2.9
-5L1M	AP-345	67.4	66.9	68.2	0.5	-0.8	-1.3
-5M1M	AP-281	68.1	65.4	66.1	2.7	2.0	-0.7
-6C1M	AP-239	67.6	70.7	71.5	-3.1	-3.9	-0.8
-6H1M	AP-400	65.5	64.7	64.5	0.8	1.0	0.2
-6L1M	AP-233	69.1	69.3	70.2	-0.2	-1.1	-0.9
-6R1M	AP-273	66.8	66.2	66.3	0.6	0.5	-0.1
-6R2M	AP-381	66.9	66.4	65.9	0.5	1.0	0.5
-6R3M	DH-760	65.7	67.0	67.0	-1.3	-1.3	0.0
-6R4M	ROW-E1	67.5	67.8	68.7	-0.3	-1.2	-0.9
-7A2M	KR-5	68.7	64.4	64.5	4.3	4.2	-0.1
-7H4M	KR-6	68.5	64.7	69.7	3.8	-1.2	-5.0
-7H5M	KP-12	70.0	72.1	72.9	-2.1	-2.9	-0.8
-8C1M	AP-265	70.1	69.6	70.9	0.5	-0.8	-1.3
-8E2M	HA-1	71.4	72.7	72.9	-1.3	-1.5	-0.2
-8F1M	AP-264	70.6	70.7	71.9	-0.1	-1.3	-1.2
-8K3M	ROW-E2	72.3	74.1	74.5	-1.8	-2.2	-0.4
-8K4M	ROW-E2A	72.7	73.1	73.6	-0.4	-0.9	-0.5
-8K5M	ROW-E2B	72.2	72.6	73.1	-0.4	-0.9	-0.5
-8K21M	WQ-4	68.2	73.4	73.8	-5.2	-5.6	-0.4
-8N1M	AP-103	71.6	72.7	72.9	-1.1	-1.3	-0.2
-8P2M	HA-3	73.2	74.7	74.9	-1.5	-1.7	-0.2
-9L3M	AP-405	68.9	70.1	72.3	-1.2	-3.4	-2.2
-9N1M	AP-255	71.2	72.8	72.7	-1.6	-1.5	0.1
-9P1M	AP-251	71.9	71.4	72.3	0.5	-0.4	-0.9
-9Q1M	AP-404	71.0	71.5	72.6	-0.5	-1.6	-1.1
-16B1M	AP-403	69.1	72.2	73.2	-3.1	-4.1	-1.0
-16F3M	ROW-E4	73.7	74.6	75.0	-0.9	-1.3	-0.4
-16F4M	ROW-E4A	73.0	74.3	74.9	-1.3	-1.9	-0.6
-16F5M	ROW-E4B	74.2	74.3	75.0	-0.1	-0.8	-0.7
-16L3M	KR-21	74.2	75.4	75.8	-1.2	-1.6	-0.4
-17A4M	ROW-E3	73.1	75.0	75.2	-1.9	-2.1	-0.2
-17B1M	AP-168	73.1	74.8	74.9	-1.7	-1.8	-0.1
-17D2M	AP-139	70.8	67.1	71.7	3.7	-0.9	-4.6
-17D3M	HA-2	71.8	71.5	72.1	0.3	-0.3	-0.6
-17E2M	KR-7	72.7	72.0	73.5	0.7	-0.8	-1.5
-17E3M	HA-4	72.7	75.1	75.5	-2.4	-2.8	-0.4
-17G4M	D9-W1	74.7	74.8	74.8	-0.1	-0.1	0.0
-17G5M	D9-W2	74.7	74.8	74.9	-0.1	-0.2	-0.1
-17G6M	D9-W3	74.8	74.8	74.9	0.0	-0.1	-0.1
-17G7M	D9-W4	75.1	74.8	74.9	0.3	0.2	-0.1

TABLE 5.-- Comparison of simulated winter-spring hydraulic heads with measured hydraulic heads averaged for winter and spring months, May 1982 to March 1985--Continued

Location No.	USBR No.	Hydraulic heads			Difference between columns		
		Average measured	Simulated using low K	Simulated using high K	1 and 2	1 and 3	2 and 3
		(1)	(2)	(3)			
8S/10E-17J3M	HA-6	76.8	75.5	75.5	1.3	1.3	0.0
-17M2M	KR-8	72.7	71.7	72.4	1.0	0.3	-0.7
-17M3M	HA-5	73.0	69.3	74.0	3.7	-1.0	-4.7
-17N3M	KP-6	73.0	69.9	71.3	3.1	1.7	-1.4
-17P1M	G-21	73.1	72.5	73.6	0.6	-0.5	-1.1
-18P1M	G-17	74.4	72.5	72.5	1.9	1.9	0.0
-20B1M	AP-122	74.4	75.2	75.5	-0.8	-1.1	-0.3
-20B2M	KR-10	74.9	75.3	75.6	-0.4	-0.7	-0.3
-20B3M	COMPOUND	75.1	75.1	75.3	0.0	-0.2	-0.2
-20B4M	KR-D4	74.9	75.2	75.5	-0.3	-0.6	-0.3
-20C1M	KR-9	73.3	73.4	73.4	-0.1	-0.1	0.0
-20C2M	KR-9A	68.7	72.7	72.8	-4.0	-4.1	-0.1
-20H2M	KR-12	74.4	75.3	75.4	-0.9	-1.0	-0.1
-20H3M	KR-D3	75.2	76.4	76.7	-1.2	-1.5	-0.3
-21B3M	KR-20	74.9	76.0	76.5	-1.1	-1.6	-0.5
-21C1M	G-36	76.2	76.4	76.8	-0.2	-0.6	-0.4
-21C2M	D2-W1	76.7	77.3	77.4	-0.6	-0.7	-0.1
-21C3M	D2-W2	76.9	76.7	77.0	0.2	-0.1	-0.3
-21C4M	D2-W3	76.9	76.6	76.9	0.3	0.0	-0.3
-21C5M	D2-W4	77.1	76.6	76.9	0.5	0.2	-0.3
-21E2M	D3S1	75.5	76.5	76.8	-1.0	-1.3	-0.3
-21F1M	D3S2	75.6	76.7	76.8	-1.1	-1.2	-0.1
-21G1M	MD-J11	75.4	76.8	77.1	-1.4	-1.7	-0.3
-21G21M	WQ-5	74.9	76.5	77.0	-1.6	-2.1	-0.5
-21H3M	KR-19	75.0	76.4	76.9	-1.4	-1.9	-0.5
-21K5M	KR-15	75.4	76.3	76.4	-0.9	-1.0	-0.1
-21K6M	D1W1	75.2	77.2	77.3	-2.0	-2.1	-0.1
-21L4M	21D4-N	75.6	72.5	76.8	3.1	-1.2	-4.3
-21N1M	KR-13	75.6	75.4	75.4	0.2	0.2	0.0
-21R1M	SEC-21	73.4	77.0	77.0	-3.6	-3.6	0.0
-22A1M	G-26	70.0	71.8	72.1	-1.8	-2.1	-0.3
-22L1M	KR-17	74.5	76.0	77.2	-1.5	-2.7	-1.2
-22M2M	AP-135	76.6	76.7	77.2	-0.1	-0.6	-0.5
-22M5M	KR-16	76.3	76.8	77.1	-0.5	-0.8	-0.3
-22M6M	KR-18	74.5	76.5	77.1	-2.0	-2.6	-0.6
-22M7M	D1S1	76.3	77.2	77.3	-0.9	-1.0	-0.1
-26P1M	26P1	74.9	76.9	79.6	-2.0	-4.7	-2.7
-27A1M	MD-J13	74.2	75.1	77.8	-0.9	-3.6	-2.7
-27A2M	27A2	74.6	75.0	77.6	-0.4	-3.0	-2.6
-27A21M	WQ-6	74.1	75.1	77.5	-1.0	-3.4	-2.4
-28C1M	KR-14	74.3	75.6	75.9	-1.3	-1.6	-0.3
-30E1M	SF-8	74.8	76.1	76.1	-1.3	-1.3	0.0
Absolute value of average difference					1.5	1.6	0.9



0 .5 1 MILE  
0 .5 1 KILOMETER

**EXPLANATION**

- 18P1M WELL AND NUMBER - See description of well-numbering system in text
- 24C2M Simulated and measured hydraulic heads are given in tables 5 and 6
- Hydrograph of well shown in figure 12
- Ⓢ KESTERSON POND AND POND NUMBER

FIGURE 11. Location of wells measured by the U.S. Bureau of Reclamation.

### Three-Year Transient Simulation

The model simulations were for a 3-year period (April 1982 to March 1985) during which water levels in Kesterson Reservoir fluctuated seasonally and duck ponds were alternately flooded and drained. During this 3-year period drainage water was placed in Kesterson Reservoir. The 3-year transient simulation was done to simulate the seasonal change in ground-water levels and flow rates. Again, two sets of values of hydraulic properties were used in separate simulations to reflect uncertainty in those data. Adjustment of hydraulic conductivities or specific yield were not made in an attempt to calibrate the model.

A measure of the reliability of a ground-water flow model is how well it simulates hydrologic conditions observed in the field. Specifically, this would include reproducing fluctuations in hydraulic head due to change in the hydrologic system or estimated recharge or discharge rates from surface-water bodies. The comparisons made between simulated results and field conditions were (1) comparing measured hydraulic head fluctuations from April 1982 to March 1985 with simulated fluctuations during the same time period, and (2) comparing simulated summer-fall hydraulic heads with summer-fall hydraulic heads averaged for April 1982 to March 1985. Except for Kesterson Reservoir, comparisons between simulated flow volumes and measured or estimated seepage in or out of any of the creeks, sloughs, canals, and duck ponds could not be made. These data were not available. Seepage estimates were compared with model results for Kesterson Reservoir.

Comparison between measured hydraulic head fluctuation for May 1982 to March 1985 with simulated hydraulic head fluctuations that correspond to the same time period are shown for 19 selected observation wells (fig. 12).

The fluctuations in simulated hydraulic heads generally coincide with measured hydraulic-head fluctuations. In most instances, the amplitude of the simulated head fluctuation is less than the fluctuation in measured head. Measured ground-water levels fluctuate in response to (1) draining and flooding the numerous duck ponds in the study area, (2) change in stage at Kesterson Reservoir, and any other surface-water body, (3) evapotranspiration, and (4) any undocumented local ground-water pumping. In the model, duck ponds were alternately drained and flooded from summer to winter, the stage at Kesterson Reservoir fluctuated seasonally, and ground-water losses from evapotranspiration were included for the summer-fall simulation. Any other stress on the ground-water flow system, such as undocumented local pumping, that might affect ground-water levels was not accounted for.

Comparisons for some instances are not very good. These discrepancies may be attributed to the model simulating average winter and summer flow conditions so that seasonal variations in stresses are not included in the simulation. Where local flow conditions, such as local variation in surface-water stage, deviate from these average flow conditions, the simulated hydraulic heads do not compare favorably with measured hydraulic heads. This is true to some extent with each of these hydrographs. Other possible reasons for the difference between measured and simulated hydraulic heads may be (1) errors in estimating the stage of duck ponds, canals and sloughs (wells 8S/9E-11C2M and 8S/10E-16F3M, -8K3M, -17A4M, -20B1M), (2) not accounting for stage fluctuations in surface-water bodies other than Kesterson Reservoir and the duck ponds (wells 8S/10E-4D1M, -9F2M, -22A1M), (3) any undocumented ground-water pumping (wells 8S/9E-11C2M, 8S/10E-21L4M), or (4) fluctuations in boundary fluxes due to stresses on the aquifer system outside the model area (wells 8S/9E-11C2M, 8S/10E-21L4M). Where hydraulic head comparisons are good, the dominant factors that affect ground-water levels have probably been accounted for.

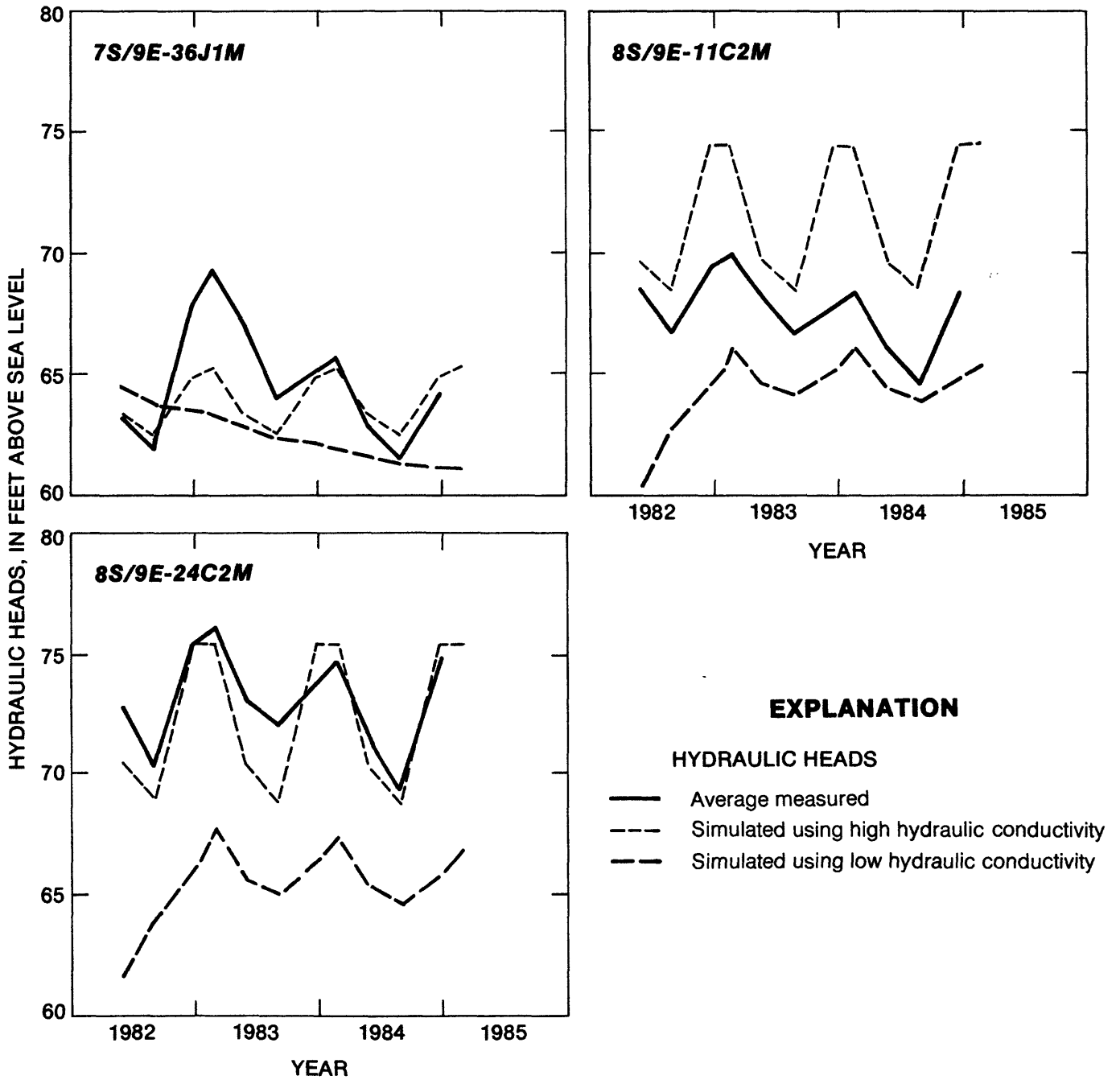


FIGURE 12. Comparison of measured and simulated hydraulic heads for selected observation wells, May 1982 to March 1985.

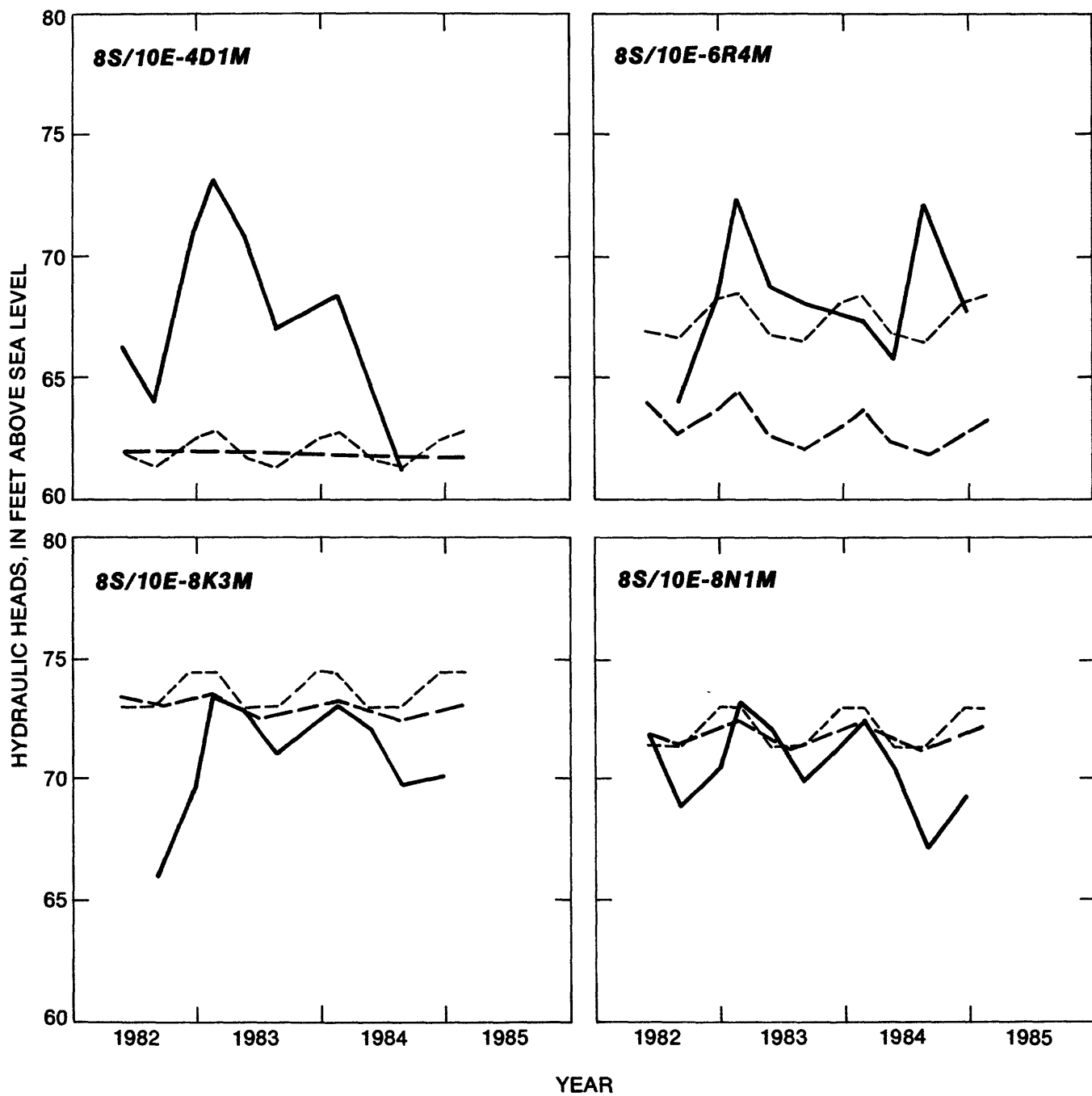


FIGURE 12. Comparison of measured and simulated hydraulic heads for selected observation wells, May 1982 to March 1985 --Continued.

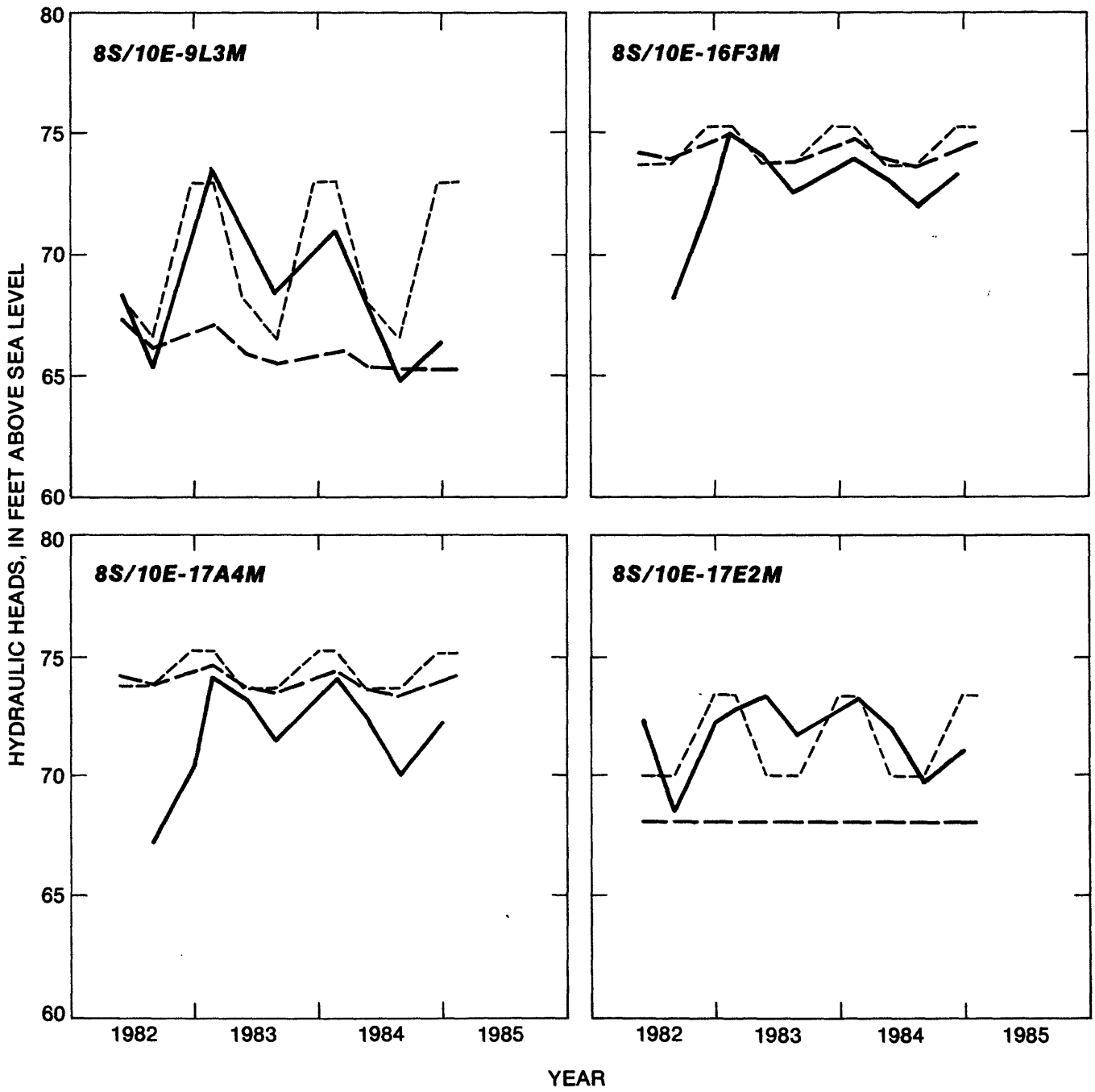


FIGURE 12. Comparison of measured and simulated hydraulic heads for selected observation wells, May 1982 to March 1985--Continued.

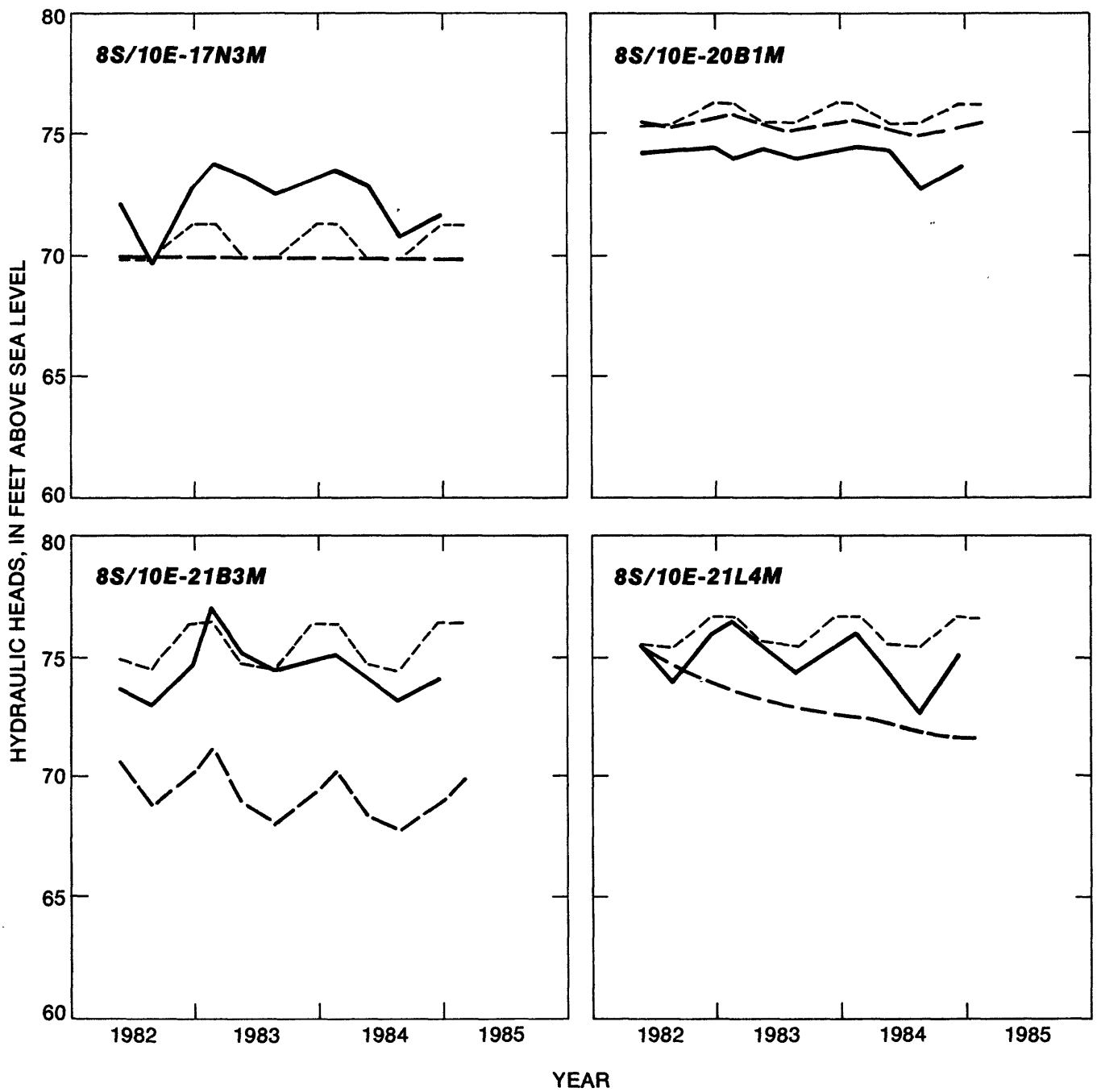


FIGURE 12. Comparison of measured and simulated hydraulic heads for selected observation wells, May 1982 to March 1985--Continued.

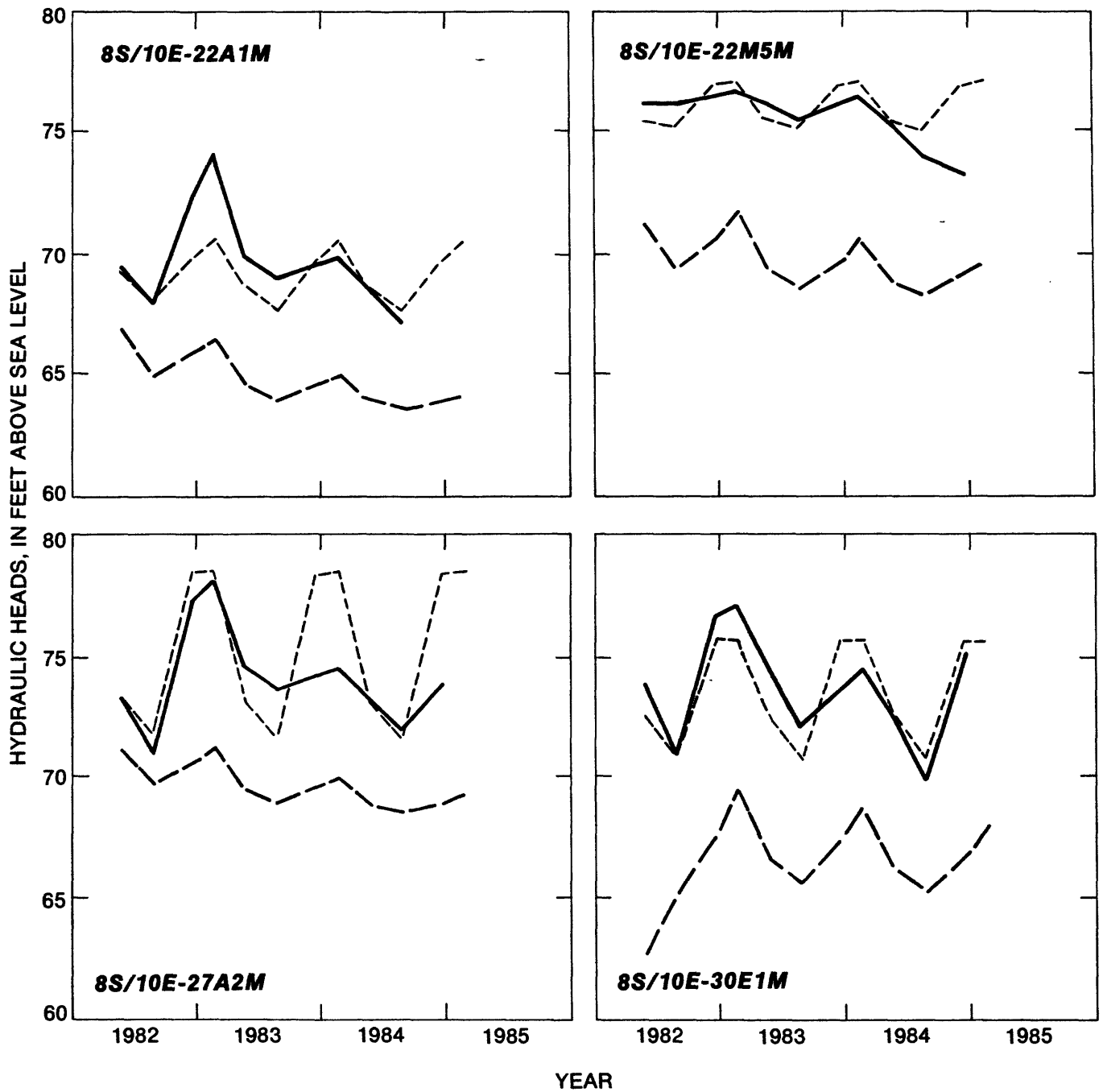


FIGURE 12. Comparison of measured and simulated hydraulic heads for selected observation wells, May 1982 to March 1985--Continued.

In general, the simulation with the high values of hydraulic conductivity match measured hydraulic-head fluctuations better than the simulation with the low values of hydraulic conductivity. The simulations with the high values of hydraulic conductivity respond much faster to changes in model stresses represented by head dependent ground-water sources or sinks. Specific yield, which was 0.10, was not varied in an attempt to improve the comparison with measured hydraulic-head fluctuations.

Comparison of these hydrographs indicates that the simulation using the high values of hydraulic conductivity generally results in a better match with measured water levels. Differences between simulated hydraulic heads for the two simulations were often greater than differences between simulated and measured heads. Errors in estimating stage altitudes and fluctuations are the probable reason for discrepancies in the amplitude and phase of the simulated hydrographs relative to the measured hydrographs and may result in errors in simulated flow directions. Uncertainty in estimating hydraulic conductivity does not always result in large variations in simulated head. However, the resulting simulated ground-water rates may vary considerably.

The only estimates of seepage fluxes between surface-water bodies and the underlying ground-water system that were made in the study area are the estimated seepage rates from Kesterson Reservoir. Documented seepage studies are not available for Mud Slough, Salt Slough, the canals in the study area, Los Banos Creek, or that part of the San Joaquin River that is included in the study area. Not only are seepage rates unknown, but the direction of seepage is unknown for all cases, since ground-water levels and surface-water stage are unknown along each of the surface-water bodies.

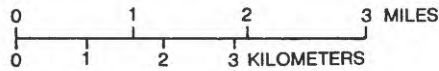
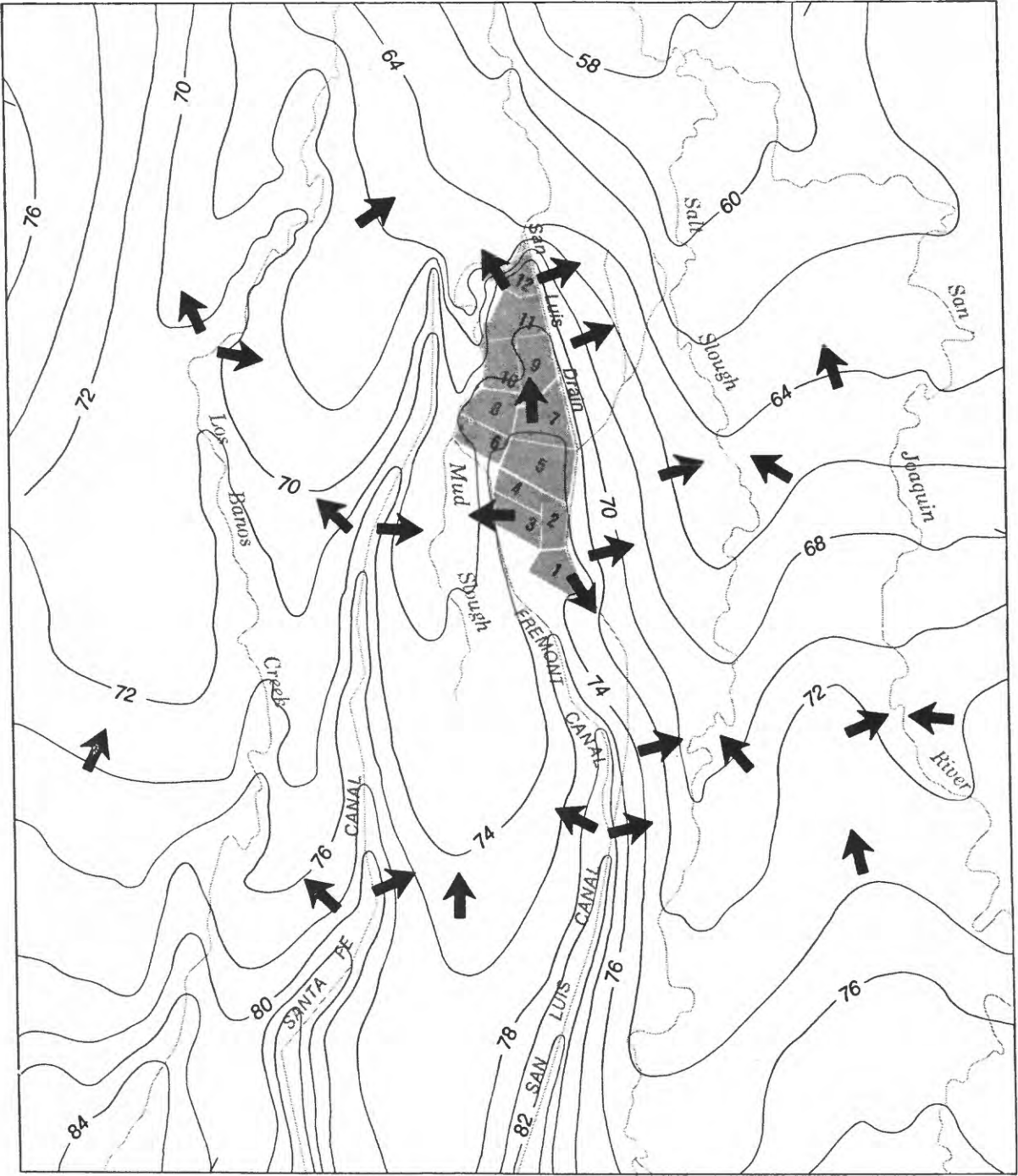
Using the low values of vertical hydraulic conductivity, the simulated seepage fluxes out of Kesterson Reservoir

were 0.22 ft/yr. Seepage fluxes of 11.68 ft/yr were calculated using the high values of vertical hydraulic conductivity. These model-estimated fluxes bracket the seepage flux estimated from measured water-budget data. The water-budget estimate of the seepage flux described earlier is  $1.4 \times 10^{-7}$  ft/s, or 3.5 ft/yr, which is in between the low and high hydraulic conductivity simulations. Because of the variability in texture of materials making up the bottom of ponds at Kesterson, variations in the rate of vertical flow will be great from different parts of these ponds. In areas where fine-grained materials predominate, the rates will be low, close to 0.22 ft/yr. In areas where there are coarse-grained deposits, the vertical flux will be closer to 11.68 ft/yr. Neither flux applies uniformly to the entire area covered by Kesterson Reservoir.

#### Simulation of Summer-Fall Flow Conditions

Ground-water flow conditions, typical of late summer and early fall in this area, were simulated during the transient simulation just described to show ground-water flow conditions when the ground-water levels are generally lowest. In the late spring, duck ponds throughout the Central Valley are drained and much of the land that was covered by these duck ponds is used as pastureland during the summer months. Water levels decline in response to the draining of duck ponds, evapotranspiration, declines in pond stages at Kesterson Reservoir, and probable declines in stage of the San Joaquin River and Mud and Salt Sloughs and any undocumented ground-water pumping. During this transient simulation, that part of the San Luis Canal that delivers water to the Kesterson Wildlife Refuge is dry and is not included.

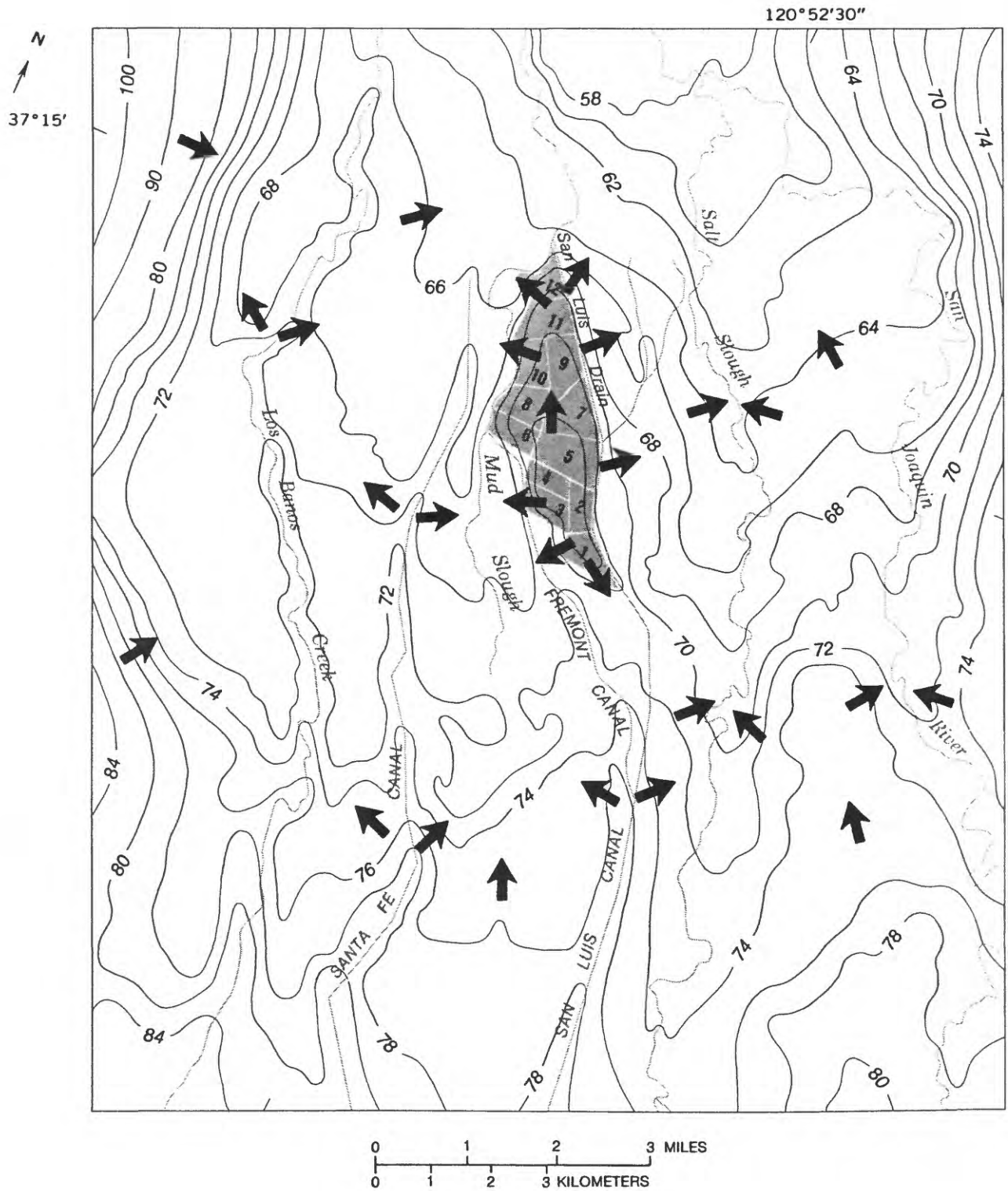
The simulated summer-fall results are shown as a map of hydraulic head for model layer 1 for the high values of hydraulic conductivity and for the low values of hydraulic conductivity (figs. 13 and 14).



**EXPLANATION**

-  SIMULATED DIRECTION OF GROUND-WATER MOVEMENT (NOT TO SCALE)
-  — 80 — LINE OF EQUAL SIMULATED HYDRAULIC HEAD, IN FEET - Interval is variable
-  4 KESTERSON POND AND POND NUMBER

FIGURE 13. Simulated hydraulic heads in model layer 1 for summer-fall flow conditions using high values of hydraulic conductivity.



**EXPLANATION**

- SIMULATED DIRECTION OF GROUND-WATER MOVEMENT (NOT TO SCALE)
- 80 — LINE OF EQUAL SIMULATED HYDRAULIC HEAD, IN FEET - Interval is variable
- 4 KESTERSON POND AND POND NUMBER

**FIGURE 14.** Simulated hydraulic heads in model layer 1 for summer-fall flow conditions using low values of hydraulic conductivity.

The simulated regional ground-water flow system is similar to the winter-spring simulation in that flow is generally from south to north. The main difference is that ground-water levels have declined regionally. The hydraulic-head gradient between the canals and the underlying aquifer has increased, indicating greater potential for water loss from these canals. The hydraulic-head gradient between Los Banos Creek and the underlying aquifer has reversed so that Los Banos Creek would be losing water during this time period. The head gradient between the underlying aquifer and Mud Slough, Salt Slough, and the San Joaquin River has decreased, indicating less ground-water discharge to these surface-water bodies.

In the low and high hydraulic conductivity simulations, Kesterson Reservoir continues to act as a source of recharge. The simulated directions of ground-water flow for both sets of hydraulic conductivity values are away from the ponds at Kesterson that have water during the summer months. The ponds at Kesterson Reservoir that generally were not operated during the summer months (ponds 3, 4, 6, 8, and 10) receive ground-water seepage from the ponds that are filled with agricultural drainage water. These simulations show that the probable source of seepage to these ponds comes from the ponds at Kesterson that are in operation and not from surrounding areas.

Flow from Kesterson Reservoir is to the east and northeast toward Salt Slough and

to the west and northwest toward Mud Slough. There is a southerly component of simulated ground-water flow from pond 1, that probably moves to the east and northeast after a very short travel distance to the south. This is evident in simulations with both values of hydraulic conductivity, but more pronounced in the simulation using the lower values of hydraulic conductivity. Salt and Mud Sloughs continue to act as local interceptors of ground-water flow. Both simulations show that ground water does not flow from Kesterson Reservoir to areas beyond Mud Slough to the west or beyond Salt Slough to the east. At Mud and Salt Sloughs, the simulated direction of ground-water flow is upward from the underlying aquifer. Simulated flow directions west of Mud Slough are predominately to the northeast toward the San Joaquin River and east toward Mud Slough. Simulated ground-water flow directions east of Salt Slough are to the north and east toward the San Joaquin River and west toward Salt Slough. The simulated flow patterns for Kesterson Reservoir are in general agreement with those inferred from measured ground-water levels (fig. 3).

Table 6 shows a comparison made between simulated and average measured hydraulic heads for summer-fall flow conditions. The average differences between measured and simulated hydraulic heads are 1.7 feet for the low values of hydraulic conductivity and 1.4 feet for the higher values of hydraulic conductivity.

TABLE 6.--Comparison of simulated summer-fall hydraulic heads with measured hydraulic heads averaged for summer and fall months, May 1982 to March 1985

Location No.	USBR No.	Hydraulic heads			Difference between columns		
		Average measured (1)	Simulated using low K (2)	Simulated using high K (3)	1 and 2	1 and 3	2 and 3
7S/9E-35JIM	AP-198	62.1	63.1	62.6	-1.0	-0.5	0.5
-35NIM	G-11	64.6	64.4	64.4	0.2	0.2	0.0
-36JIM	ER-81M	62.9	62.3	61.9	0.6	1.0	0.4

TABLE 6.--Comparison of simulated summer-fall hydraulic heads with measured hydraulic heads averaged for summer and fall months, May 1982 to March 1985--Continued

Location No.	USBR No.	Hydraulic heads			Difference between columns		
		Average measured	Simulated using low K	Simulated using high K	1 and 2	1 and 3	2 and 3
		(1)	(2)	(3)			
7S/9E-36L1M	ID-513	61.7	62.9	62.0	-1.2	-0.3	0.9
-36N2M	AP-205	62.7	63.9	63.1	-1.2	-0.4	0.8
-36N3M	DH-754	64.4	64.5	62.9	-0.1	1.5	1.6
7S/10E-31B1M	AP-325	60.5	54.6	58.1	5.9	2.4	-3.5
-31C1M	AP-324	60.2	58.0	58.8	2.2	1.4	-0.8
-31H1M	AP-307	60.6	58.1	58.8	2.5	1.8	-0.7
-31N1M	AP-300	54.7	62.4	62.1	-7.7	-7.4	0.3
-32C1M	32C1	61.2	59.0	58.6	2.2	2.6	0.4
-32F1M	G-14	61.2	60.3	59.6	0.9	1.6	0.7
-32Q1M	ER-76G	64.7	60.6	60.3	4.1	4.4	0.3
8S/9E-11C2M	SF-2	66.5	67.2	67.9	-0.7	-1.4	-0.7
-24C2M	SF-6A	71.1	64.0	68.3	7.1	2.8	-4.3
8S/10E-4D1M	4D1	64.2	61.2	60.7	3.0	3.5	0.5
-4L1M	AP-249	64.7	62.2	61.5	2.5	3.2	0.7
-4M1M	AP-277	64.2	63.5	62.9	0.7	1.3	0.6
-4M2M	AP-407	64.3	62.2	61.6	2.1	2.7	0.6
-5A1M	AP-247	64.2	61.1	60.7	3.1	3.5	0.4
-5E1M	AP-284	62.9	62.8	62.8	0.1	0.1	0.0
-5G1M	AP-285	63.5	62.5	62.5	1.0	1.0	0.0
-5K1M	AP-346	64.6	63.9	64.1	0.7	0.5	-0.2
-5L1M	AP-345	64.4	64.1	64.6	0.3	-0.2	-0.5
-5M1M	AP-281	64.1	61.1	63.2	3.0	0.9	-2.1
-6C1M	AP-239	63.1	59.8	62.8	3.3	0.3	-3.0
-6H1M	AP-400	62.1	63.4	63.0	-1.3	-0.9	0.4
-6L1M	AP-233	65.0	63.8	63.4	1.2	1.6	0.4
-6R1M	AP-273	64.2	62.1	64.1	2.1	0.1	-2.0
-6R2M	AP-381	65.0	64.3	64.0	0.7	1.0	0.3
-6R3M	DH-760	63.4	65.0	64.6	-1.6	-1.2	0.4
-6R4M	ROW-E1	65.2	61.6	65.9	3.6	-0.7	-4.3
-7A2M	KR-5	66.0	63.8	63.8	2.2	2.2	0.0
-7H4M	KR-6	65.7	64.0	64.5	1.7	1.2	-0.5
-7H5M	KP-12	66.5	70.2	70.5	-3.7	-4.0	-0.3
-8C1M	AP-265	66.2	66.4	67.5	-0.2	-1.3	-1.1
-8E2M	HA-1	68.8	70.6	70.5	-1.8	-1.7	0.1
-8F1M	AP-264	68.4	64.8	68.0	3.6	0.4	-3.2
-8K3M	ROW-E2	68.6	72.0	72.3	-3.4	-3.7	-0.3
-8K4M	ROW-E2A	69.1	70.7	70.9	-1.6	-1.8	-0.2
-8K5M	ROW-E2B	70.0	69.9	70.3	0.1	-0.3	-0.4
-8K21M	WQ-4	65.9	71.1	71.2	-5.2	-5.3	-0.1
-8N1M	AP-103	68.4	70.6	70.6	-2.2	-2.2	0.0
-8P2M	HA-3	70.5	72.1	71.9	-1.6	-1.4	0.2
-9L3M	AP-405	66.2	66.2	65.9	0.0	0.3	0.3
-9N1M	AP-255	67.5	67.2	69.5	0.3	-2.0	-2.3
-9P1M	AP-251	67.7	65.9	66.7	1.8	1.0	-0.8

TABLE 6.--Comparison of simulated summer-fall hydraulic heads with measured hydraulic heads averaged for summer and fall months, May 1982 to March 1985--Continued

Location No.	USBR No.	Hydraulic heads			Difference between columns		
		Average measured	Simulated using low K	Simulated using high K	1 and 2	1 and 3	2 and 3
		(1)	(2)	(3)			
8S/10E-9Q1M	AP-404	67.1	67.0	67.3	0.1	-0.2	-0.3
-16B1M	AP-403	67.0	67.5	68.4	-0.5	-1.4	-0.9
-16F3M	ROW-E4	71.1	72.4	72.5	-1.3	-1.4	-0.1
-16F4M	ROW-E4A	70.6	71.0	71.8	-0.4	-1.2	-0.8
-16F5M	ROW-E4B	72.6	70.3	71.8	2.3	0.8	-1.5
-16L3M	KR-21	72.1	73.1	73.7	-1.0	-1.6	-0.6
-17A4M	ROW-E3	69.6	72.8	73.0	-3.2	-3.4	-0.2
-17B1M	AP-168	70.6	72.2	71.9	-1.6	-1.3	0.3
-17D2M	AP-139	68.6	66.4	67.3	2.2	1.3	-0.9
-17D3M	HA-2	69.3	69.6	69.6	-0.3	-0.3	0.0
-17E2M	KR-7	70.4	69.9	70.3	0.5	0.1	-0.4
-17E3M	HA-4	71.0	72.9	73.1	-1.9	-2.1	-0.2
-17G4M	D9-W1	73.6	73.4	72.5	0.2	1.1	0.9
-17G5M	D9-W2	73.6	73.5	72.5	0.1	1.1	1.0
-17G6M	D9-W3	73.5	73.5	72.5	0.0	1.0	1.0
-17G7M	D9-W4	73.5	73.5	72.5	0.0	1.0	1.0
-17J3M	HA-6	75.0	73.4	73.1	1.6	1.9	0.3
-17M2M	KR-8	71.0	69.1	70.0	1.9	1.0	-0.9
-17M3M	HA-5	71.8	68.5	71.1	3.3	0.7	-2.6
-17N3M	KP-6	71.4	69.2	69.2	2.2	2.2	0.0
-17P1M	G-21	71.5	69.9	71.5	1.6	0.0	-1.6
-18P1M	G-17	72.0	66.3	68.8	5.7	3.2	-2.5
-20B1M	AP-122	73.9	73.0	74.1	0.9	-0.2	-1.1
-20B2M	KR-10	73.7	73.6	73.7	0.1	0.0	-0.1
-20B3M	COMPOUND	74.2	73.1	73.8	1.1	0.4	-0.7
-20B4M	KR-D4	74.4	73.0	74.1	1.4	0.3	-1.1
-20C1M	KR-9	71.6	70.9	71.6	0.7	0.0	-0.7
-20C2M	KR-9A	67.7	68.7	71.0	-1.0	-3.3	-2.3
-20H2M	KR-12	73.0	72.5	73.9	0.5	-0.9	-1.4
-20H3M	KR-D3	74.4	74.4	74.7	0.0	-0.3	-0.3
-21B3M	KR-20	73.4	72.1	73.8	1.3	-0.4	-1.7
-21C1M	G-36	76.2	74.5	75.0	1.7	1.2	-0.5
-21C2M	D2-W1	75.8	75.9	75.9	-0.1	-0.1	0.0
-21C3M	D2-W2	75.8	75.4	75.3	0.4	0.5	0.1
-21C4M	D2-W3	75.7	75.4	75.2	0.3	0.5	0.2
-21C5M	D2-W4	75.6	75.4	75.2	0.2	0.4	0.2
-21E2M	D3S1	73.8	74.6	74.7	-0.8	-0.9	-0.1
-21F1M	D3S2	74.6	74.8	74.7	-0.2	-0.1	0.1
-21G1M	MD-J11	74.5	74.6	75.3	-0.1	-0.8	-0.7
-21G21M	WQ-5	74.0	74.4	75.0	-0.4	-1.0	-0.6
-21H3M	KR-19	73.8	72.1	74.3	1.7	-0.5	-2.2
-21K5M	KR-15	74.1	71.5	74.6	2.6	-0.5	-3.1
-21K6M	D1W1	74.7	75.4	75.8	-0.7	-1.1	-0.4
-21L4M	21D4-N	74.0	69.3	66.4	4.7	7.6	2.9

TABLE 6.--Comparison of simulated summer-fall hydraulic heads with measured hydraulic heads averaged for summer and fall months, May 1982 to March 1985--Continued

Location No.	USBR No.	Hydraulic heads			Difference between columns		
		Average measured	Simulated using low K	Simulated using high K	1 and 2	1 and 3	2 and 3
		(1)	(2)	(3)			
8S/10E-21N1M	KR-13	74.1	71.6	74.2	2.5	-0.1	-2.6
-21R1M	SEC-21	71.7	66.4	74.3	5.3	-2.6	-7.9
-22A1M	G-26	68.0	63.5	67.1	4.5	0.9	-3.6
-22L1M	KR-17	72.5	69.8	72.1	2.7	0.4	-2.3
-22M2M	AP-135	76.1	73.3	74.8	2.8	1.3	-1.5
-22M5M	KR-16	74.9	72.4	74.5	2.5	0.4	-2.1
-22M6M	KR-18	72.9	73.5	74.9	-0.6	-2.0	-1.4
-22M7M	D1S1	75.3	75.6	75.8	-0.3	-0.5	-0.2
-26P1M	26P1	74.5	73.7	76.2	0.8	-1.7	-2.5
-27A1M	MD-J13	72.8	71.1	71.2	1.7	1.6	-0.1
-27A2M	27A2	72.6	71.0	71.0	1.6	1.6	0.0
-27A21M	WQ-6	72.1	71.6	71.3	0.5	0.8	0.3
-28C1M	KR-14	72.2	71.7	74.4	0.5	-2.2	-2.7
-30E1M	SF-8	71.6	69.6	70.2	2.0	1.4	-0.6
Absolute value of average difference					1.7	1.4	1.0

#### ESTIMATING GROUND-WATER FLOW DIRECTION AND TRAVELTIME

A nonreactive constituent dissolved in ground water will generally move with ground water and, on the average, travel from one point to another in the same amount of time as the ground water. Therefore a useful first step in assessing the potential for contaminant transport from Kesterson Reservoir is to estimate ground-water traveltimes and distances. Since most contaminants are not conservative, this type of assessment is an estimate of the most rapid movement of contaminants traveling at the average linear, or pore, velocity. This analysis ignores the effects of dispersion and diffusion on contaminant movement. First order approximations of ground-water traveltimes and travel distances using volumetric fluxes can be made with the ground-water flow model. In this type of

analysis, only average ground-water flow paths are approximated. The result of this analysis would represent some average ground-water traveltime for a non-reactive dissolved constituent, since minimum and maximum pore velocities have not been accounted for.

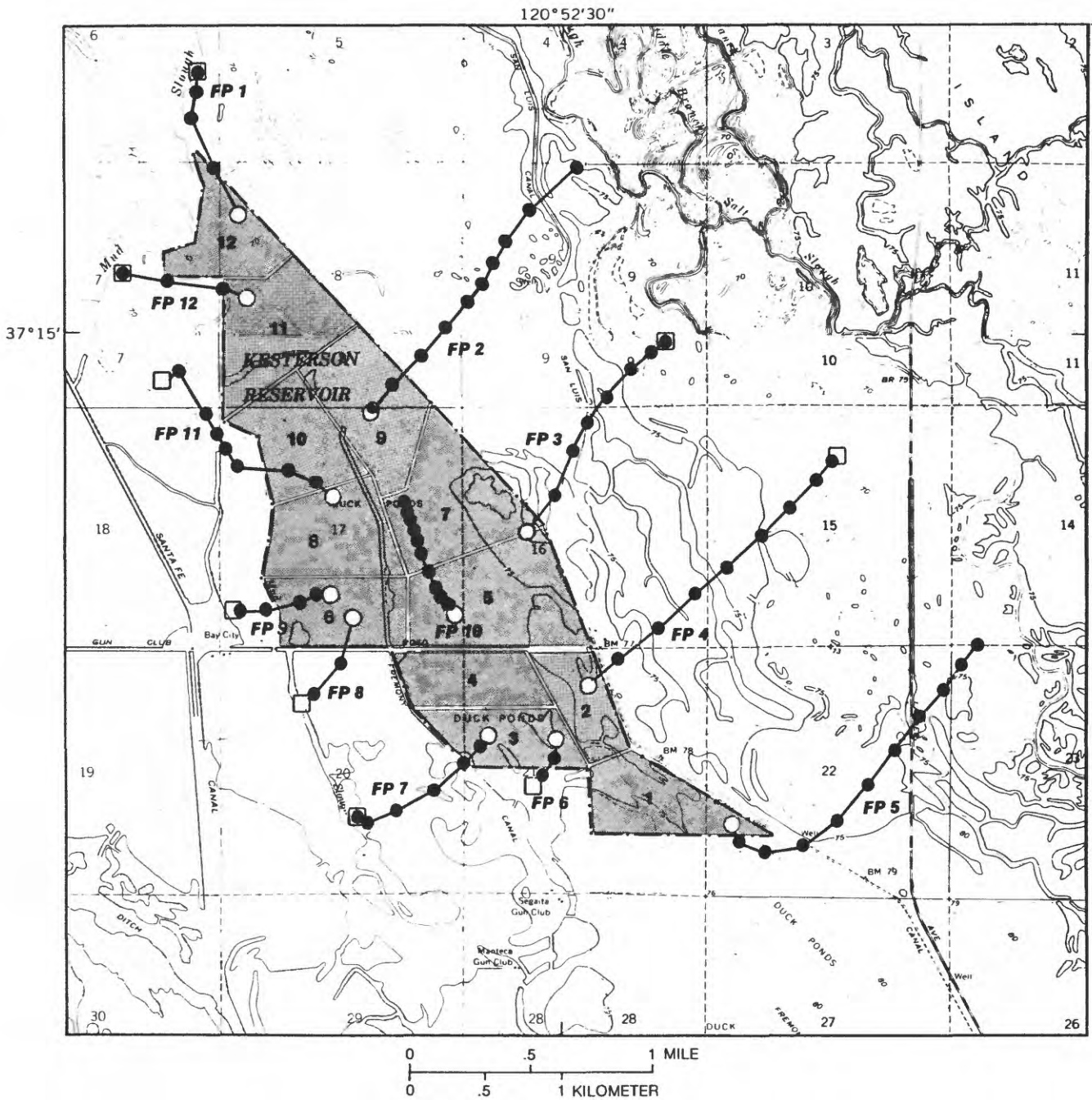
Ground-water flow conditions follow a seasonal cycle that repeats itself year after year. This seems to be verified by measured water levels from observation wells in the vicinity. For the flow direction and traveltime approximations, average annual flow rates were used instead of cycling from winter-flow rates to summer-flow rates for several years. The average between winter and summer ground-water flow rates should approximate long-term flow rates, provided that the ground-water flow system does not radically change from the one that has been depicted.

The method of approximating travel distances uses volumetric fluxes from the three-dimensional ground-water flow model (McDonald and Harbaugh, 1984). Briefly, the volumetric flux is divided by the area perpendicular to flow to calculate specific discharge. Specific discharge is then divided by the estimated effective porosity to get average linear or pore velocity. This is done for all ground-water flow components in each of the x, y, and z directions at each model node. The x, y, and z components of pore velocity at any location other than at a node are calculated by linear interpolation between surrounding nodes in three dimensions. The distance traveled in the x, y, and z direction for a given time period are calculated by multiplying pore velocity by time period length. Details of the method used to estimate travel distances are included in Appendix A.

Estimates of effective porosity of the unconsolidated continental or flood-plain deposits are not available for the Kesterson area. Johnson and others (1968) determined total porosity for 523 samples taken from wells on the west side of the San Joaquin Valley. The average porosity from these samples was 40 percent. Effective porosity will be less than total porosity because of the effect of non-interconnected pores. Exactly how much less is uncertain. In estimating travel distances, average total porosity was used. This will result in underestimating average pore velocities. As an example, if effective porosity was actually 20 percent, the average pore velocities would be twice as fast as those calculated using 40 percent. Therefore, there is a fairly high potential for error in the following analysis, with errors most likely to be made in the direction of underestimating pore velocity for a particular hydraulic conductivity.

Flow patterns from Kesterson Reservoir are shown in figures 15 and 16. Only the flow paths for the simulation using the higher values of hydraulic conductivity are shown. The distances traveled using the low values of hydraulic conductivity were small, such as would occur through clayey materials. This condition seems to be unrealistic for the sandy material above the E clay. The average pore velocities were only 0.01 ft/yr in the horizontal and vertical directions for low conductivity simulations. For the high conductivity simulations, the average pore velocity for horizontal movement was 140 ft/yr and for vertical movement, 14.7 ft/yr. The flow direction and velocity analysis was carried out for a simulated time period of 100 years. The analysis relies on the assumption that ground-water flow conditions will not differ substantially from the average conditions simulated by the model.

Simulated ground-water flow paths do not extend beyond Mud Slough to the east, nor do they extend to Salt Slough to the east (fig. 15). The simulated flow paths along the west side of Kesterson Reservoir are downward from the reservoir into the underlying aquifer and then laterally toward Mud Slough where it discharges. These flow paths are relatively short. Simulated flow paths on the east side of Kesterson Reservoir are also downward from the reservoir into the underlying aquifer. The direction of flow is then northeast toward Salt Slough. Evapotranspiration causes upward ground-water fluxes between Kesterson Reservoir and Salt Slough. The result is that most ground water discharges at land surface before reaching Salt Slough. Simulated travel paths to the south are short because of regional ground-water flow from south to north and because of the effect of evapotranspiration which causes ground water to discharge at land surface.



**EXPLANATION**

-  **FP 1** FLOW PATH AND NUMBER - Each data point is equivalent to 10 years. Simulation used high values of hydraulic conductivity
-  **1** KESTERSON POND AND POND NUMBER
-  STARTING LOCATION FOR SIMULATION
-  POINT AT WHICH FLOW PATH TERMINATES AT LAND SURFACE
-  BOUNDARY OF KESTERSON PONDS

FIGURE 15. Directions and rates of ground-water flow from Kesterson Reservoir along selected flow paths.

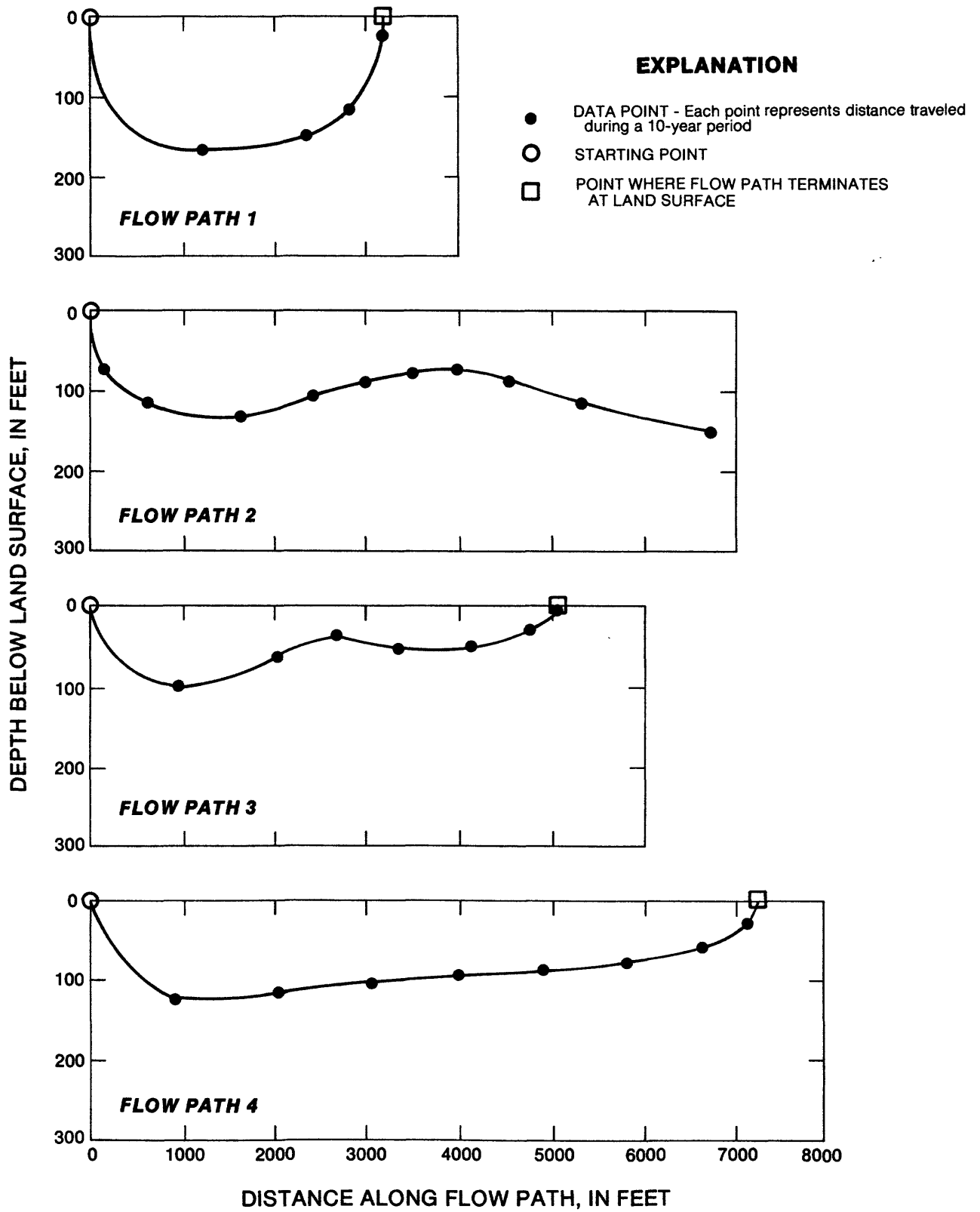


FIGURE 16. Travel distances along flow paths 1 through 12.

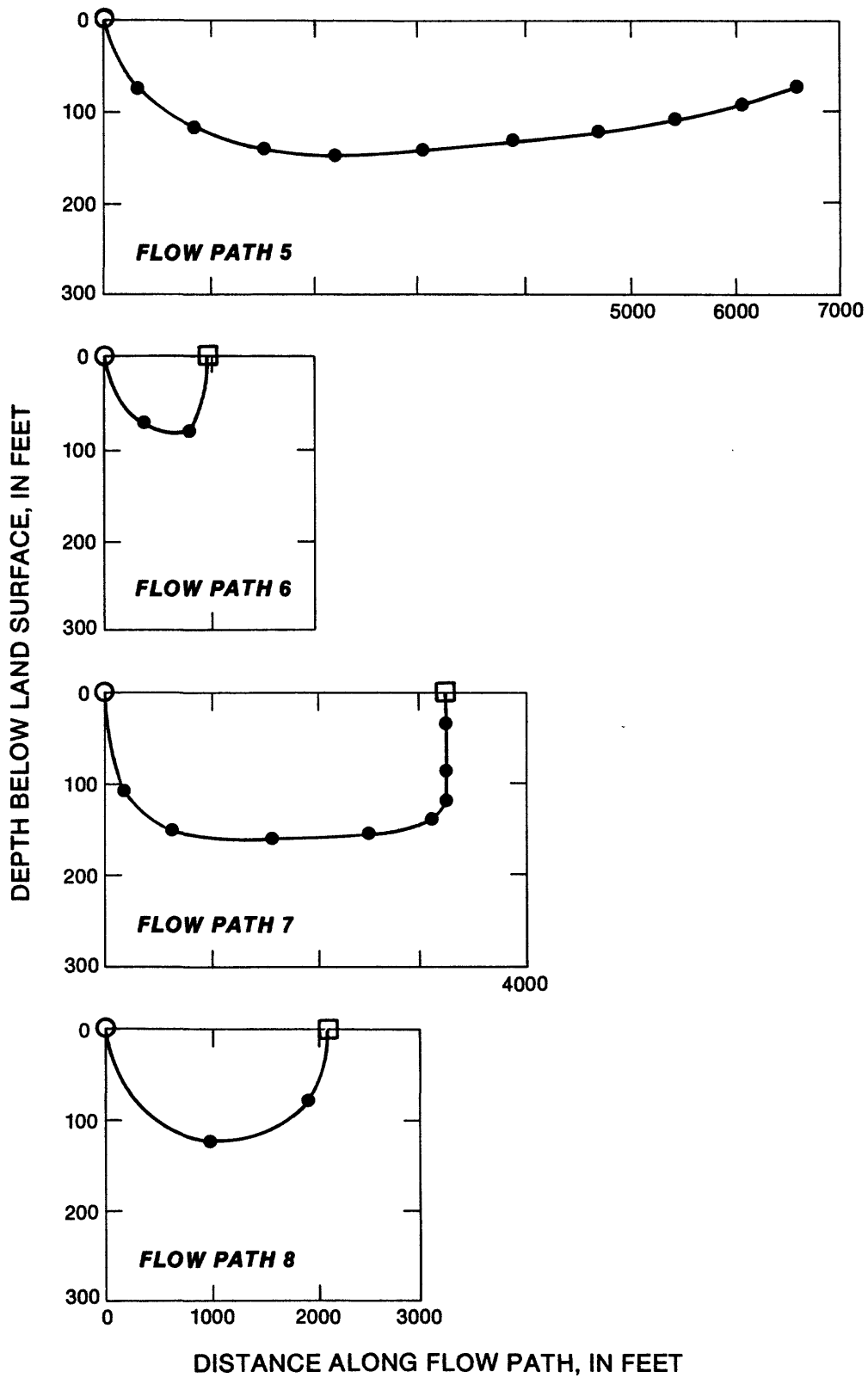


FIGURE 16. Travel distances along flow paths 1 through 12--Continued.

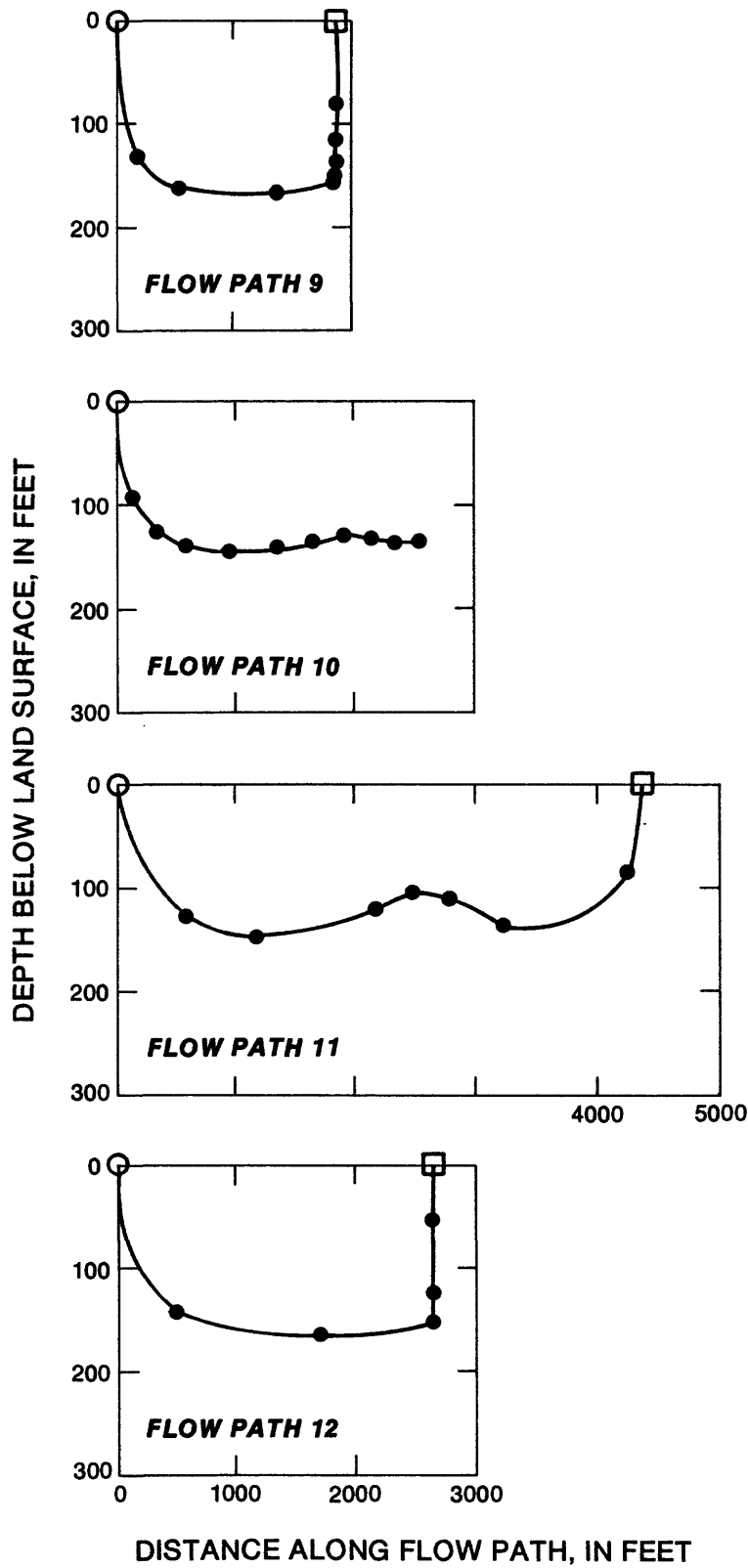


FIGURE 16. Travel distances along flow paths 1 through 12--Continued.

## MODEL LIMITATIONS

All mathematical models which simulate natural systems have basic limitations when applied to hydrologic assessment. These limitations result from such factors as oversimplification imposed by model assumptions and insufficient data to reliably evaluate model accuracy. Important limitations of the model described in this report, which should be carefully considered by those interpreting model results, are listed below.

(1) The hydrologic system has been subdivided into discrete space and time increments. The minimum model grid spacing is 500 feet and the minimum time step size is 3 months. Hydrologic conditions are spatially averaged for each finite-difference block and averaged with time for each time step. Ground-water flow conditions that occur on space and time scales that are smaller than these cannot be simulated with this model.

(2) The unconsolidated continental and flood-plain deposits have been combined into three layers, each with uniform hydraulic properties. In reality, heterogeneities in these deposits will cause ground water to flow at different rates within each model layer. This will result in differential movement of water that seeps into the ground-water flow system from Kesterson. To investigate the likely range of flow rates in the real system, the vertical and horizontal hydraulic conductivity were varied for the range of values from field tests. This was a simple attempt to account for the possible influence of the heterogeneity of these deposits.

(3) This model is not calibrated. Model results must be viewed as only an approximation of ground-water flow conditions in this area. The large number of head-dependent functions in this model tend to force simulated heads to approximate regional trends and fluctuations in the fixed heads in those head-dependent functions. This is true to some extent even with different values of hydraulic conductivity. As a result, comparing

simulated hydraulic heads and measured ground-water levels is not an adequate test of the accuracy of the model. Simulated flow rates need to be compared with measured or estimated flow rates. This was not done for the duck ponds, sloughs, creeks, and canals since independent estimates of flow rates were not available. Comparisons were made for Kesterson Reservoir.

(4) The accuracy of the simulation results is highly dependent on the reliability of model input data. The data required by the model were derived from field measurements or estimated from other sources of information. Values of horizontal and vertical hydraulic conductivity were varied over the range of values estimated from field studies. Errors in estimating the range in hydraulic conductivity will result in greater errors in simulated ground-water flow rates than in simulated hydraulic heads. Ratios of horizontal to vertical conductivity greater than 10 to 1 will result in less vertical flow. Lower ratios will result in more vertical flow. Water levels and fluctuations were known only for Kesterson Reservoir. Other stage data required in the model were estimated. An attempt was not made to account for fluctuations in stages with time. Error in estimating water levels or not accounting for real seasonal fluctuations in water levels will result in error in calculating ground-water flow rates. More importantly, simulated local flow directions possibly could be in error because of errors in relative head differences between duck ponds, canals, sloughs, and the ponds at Kesterson Reservoir. Errors in estimating effective porosity will directly affect calculated velocities. As an example, if effective porosity was 20 percent instead of 40 percent, the calculated pore velocities would be twice as fast.

(5) The model program used in this study simulates hydraulic heads and ground-water flow rates in three dimensions. The governing equation that is solved does not include the transport of solutes. But, if the solute is non-

reactive and the ground-water flow model is calibrated, so that pore velocities are known, the results of the flow model may be used to approximate average contaminant travel velocities and flow paths. Such an approximation does not include the effects of dispersion and diffusion on the contaminant concentration. As a result, the flow-path analysis in this report does not necessarily approximate the first arrival time of the contaminant. In order to accurately simulate non-reactive contaminant transport, ground-water pore velocities must be accurate. This requires a better definition of sand and clay lenses in the aquifer, knowledge of the effective porosity of the material the contaminant flows through, and a knowledge of the horizontal and longitudinal dispersivity of the porous media. For reactive contaminants, it is necessary to determine the chemistry of species of interest in an aqueous solution in the presence of different dissolved ions, and in solid-phase minerals.

## SUMMARY AND CONCLUSIONS

A three-dimensional ground-water flow model was used to simulate ground-water flow in the vicinity of Kesterson Reservoir in the San Joaquin Valley, California. The purpose of this study was to use available data to calculate a probable range of ground-water flow rates and directions of ground-water flow. The model was not calibrated or tested by comprehensive sensitivity analysis.

The model was used to simulate hydraulic heads and ground-water flow rates for (1) ground-water flow conditions typical of winter-spring months during which ground-water levels are highest, (2) a 3-year period during which agricultural drainage water flowed into Kesterson Reservoir, and (3) average ground-water conditions measured during summer-fall months during which ground-water levels generally are at their lowest level.

Flow directions, as inferred from measured hydraulic head data and simulated hydraulic heads from all model simulations, show that regional ground-water flow is from the south to north. Kesterson Reservoir acts as a recharge mound superimposed on the regional-flow system. Ground water moves in the horizontal and vertical direction away from Kesterson Reservoir. Mud and Salt Sloughs act as ground-water discharge sites. The simulations indicate that water does not flow from Kesterson Reservoir beyond either of these sloughs. Ground water from west of Mud Slough seems to flow west toward Los Banos Creek and east toward Mud Slough. Ground water between Salt Slough and the San Joaquin River appears to flow north and toward Salt Slough and the San Joaquin River, but the part that moves toward Salt Slough probably discharges at the land surface before reaching the slough. The canals and duck ponds generally act as sources of ground-water recharge.

First-order approximations of average ground-water travel times and travel distances away from Kesterson Reservoir for a nonreactive dissolved constituent were made using volumetric fluxes from the ground-water flow model. Using a range of hydraulic conductivities, a range of volumetric fluxes were calculated. These volumetric fluxes represent approximate long-term average flow conditions for a given set of hydraulic conductivity values. The flow direction and velocity analyses were carried out for a simulated time period of 100 years. This analysis assumes that ground-water flow conditions will not differ substantially from the average conditions simulated by the model.

The results show movement away from Kesterson Reservoir in all directions. The direction of all simulated flow paths are downward from the reservoirs to the underlying shallow aquifer system. Along the west side of Kesterson Reservoir, flow paths are relatively short.

Movement is toward Mud Slough where ground water discharges. Along the east side of the reservoir, flow is toward Salt Slough. Between Kesterson Reservoir and Salt Slough, evapotranspiration of ground water near the land surface causes upward ground-water flow. The result is that most ground water from Kesterson is lost by evapotranspiration before reaching Salt Slough. Simulated travel paths to the south are short because of regional ground-water flow from south to north and because of discharge of ground water near the land surface because of evapotranspiration.

#### SELECTED REFERENCES

- Croft, M.G., 1972, Subsurface geology of the late Tertiary and Quaternary water-bearing deposits of the San Joaquin Valley, California: U.S. Geological Survey Water-Supply Paper 1999-H, 29 p.
- Davis, G.H., Green, J.H., Olmsted, F.H., and Brown, D.W., 1959, Ground-water conditions and storage capacity in the San Joaquin Valley, California: U.S. Geological Survey Water-Supply Paper 1469, 187 p.
- Davis, G.H., Lofgren, B.E., and Mack, Seymour, 1964, Use of ground-water reservoirs for storage of surface water in the San Joaquin Valley, California: U.S. Geological Survey Water-Supply Paper 1618, 125 p.
- Davis, G.H., and Poland, J.F., 1957, Ground-water conditions in the Mendota-Huron area, Fresno and Kings Counties, California: U.S. Geological Survey Water-Supply Paper 1360-G, p. 409-588.
- Freeze, R.A., and Cherry, J.A., 1979, Groundwater: Englewood Cliffs, Prentice-Hall, Inc., Englewood Cliffs, N.J., 604 p.
- Huyakorn, P.S., and Pinder, G.F., 1983, Computational methods in subsurface flow: New York, Academic Press, 473 p.
- Hotchkiss, W.R., and Balding, G.O., 1971, Geology, hydrology, and water quality of the Tracy-Dos Palos area, San Joaquin Valley, California: U.S. Geological Survey Open-File Report, 107 p.
- Johnson, A.I., Moston, R.P., and Morris, D.A., 1968, Physical and hydrologic properties of water-bearing deposits in subsiding areas in central California: U.S. Geological Survey Professional Paper 497-A, 71 p.
- Kuiper, L.K., 1981, A comparison of the incomplete Cholesky-Conjugate gradient method with the strongly implicit method as applied to the solution of two-dimensional groundwater flow equations, Water Resources Research, v. 17, no. 4, p. 1082-1086.

- Lettis, W.R., 1982, Late Cenozoic stratigraphy and structure of the western margin of the central San Joaquin Valley, California: U.S. Geological Survey Open-File Report 82-526, 203 p.
- Londquist, C.L., 1981, Digital model of the unconsolidated aquifer system in the Modesto area, Stanislaus and San Joaquin Counties, California: U.S. Geological Survey Water-Resources Investigations 81-12, 36 p.
- McDonald, M.G., and Harbaugh, A.W., 1984, A modular three-dimensional finite-difference ground-water flow model: U.S. Geological Survey Open-File Report 83-875, 528 p.
- Mendenhall, W.C., Dole, R.B., and Stabler, Herman, 1916, Ground water in the San Joaquin Valley, California: U.S. Geological Survey Water-Supply Paper 398, 310 p.
- Miller, R.E., Green, J.H., and Davis, G.H., 1971, Geology of the compacting deposits in the Los Banos-Kettleman City subsidence area, California: U.S. Geological Survey Professional Paper 497-E, 46 p.
- Olson, R.E., and Daniel, D.E., 1981, Measurement of the hydraulic conductivity of fine-grained soils: Permeability and Ground-Water Contamination Transport, ASTM STP 746, T.F. Zimmie and C.O. Riggs, eds., American Society for Testing and Materials, pp. 18-64.
- Page, B.M., 1966, Geology of the Coast Ranges of California, chapter 6 of Geology of northern California: California Division of Mines Bulletin 190, p. 255-276.
- Page, R.W., 1973, Base of fresh ground water (approximately 3,000 micromhos) in the San Joaquin Valley, California: U.S. Geological Survey Hydrologic Investigations Atlas HA-489.
- 1977, Guide for data collection to calibrate a predictive digital ground-water model of the unconfined aquifer in and near the city of Modesto, California: U.S. Geological Survey Water-Resources Investigation 76-41, 46 p.
- U.S. Bureau of Reclamation, 1984, Kes-terson Reservoir and waterfowl: Information Bulletin 2, 11 p.
- U.S. Department of the Interior, Bureau of Reclamation, 1978, Drainage Manual A Water Resources Technical Publication: U.S. Department of the Interior, 286 p.
- Williamson, A.K., 1982, Evapotranspiration of applied water, Central Valley, California, 1957-78: U.S. Geological Survey Water-Resources Investigation 81-45, 56 p.
- Williamson, A.K., Prudic, D.E., and Swain, L.A., 1985, Ground-water flow in the Central Valley, California: U.S. Geological Survey Open-File Report 85-345, 203 p.

## APPENDIX A

### Calculating Travel Distances

Rough approximations of ground-water travel times and travel distances may be made using volumetric fluxes from a finite-difference ground-water flow model. In this type of approximation only advective transport is assumed. Dispersion and diffusion are not accounted for.

Flow rates calculated by the three-dimensional ground-water flow model (McDonald and Harbaugh, 1984) for each finite-difference block, are between nodes  $i,j,k$  and  $i+1,j,k$ ;  $i,j,k$  and  $i,j+1,k$ ; and  $i,j,k$  and  $i,j,k+1$ . These flow rates are actually through the finite-difference block face that separate these nodes. The first assumption made is to assign the flow rates through faces  $i+1/2,j,k$ ,  $i,j+1/2,k$  and  $i,j,k+1/2$  to node  $i,j,k$ . These flow rates then represent the volumetric flux in the  $x,y$  and  $z$  directions. Thus, at every finite difference node, the component of ground-water flow in the  $x,y$  and  $z$  direction is known. The relationship between volumetric flux through block faces and the components of flow assigned to a node are shown in figures 17a and 17b. Note that positive  $Q_y$  is in the negative  $y$ -axis direction and that  $z$  is defined as being positive downward.

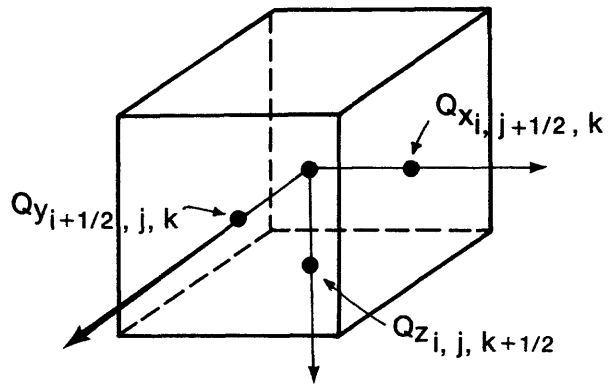
To calculate Darcian velocity or specific discharge at each node, the volumetric flux is divided by the cross-sectional area to flow.

$$q_{x_{i,j,k}} = Q_{x_{i,j,k}} / \Delta y_j * \Delta z_k \quad (6a)$$

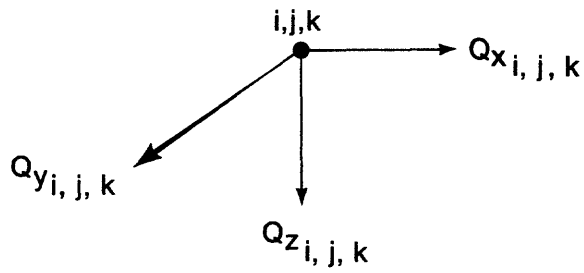
$$q_{y_{i,j,k}} = Q_{y_{i,j,k}} / \Delta x_i * \Delta z_k \quad (6b)$$

$$q_{z_{i,j,k}} = Q_{z_{i,j,k}} / \Delta x_i * \Delta y_j \quad (6c)$$

It should be possible to calculate components of specific discharge in the  $x,y$  and  $z$  directions for any  $x,y$  and  $z$  by interpolating between known values of  $q_x, q_y, q_z$  at each finite difference node.



a) Finite-difference block faces



b) Finite-difference nodes

FIGURE 17. Relation of volumetric fluxes to finite-difference block faces and finite-difference nodes.

The method that is proposed makes use of linear interpolation in three dimensions. The value of a parameter at any location  $x,y,z$  can be found using the following expression (Huyakorn and Pinder, 1983, p. 81, eq. 3.4.2.5a)

$$f(x,y,z) = \sum_{k=1}^8 N_k(x,y,z) f(x_k, y_k, z_k) \quad (7)$$

where

$N_k(x,y,z)$  are basis functions for the 8 surrounding nodes evaluated at location  $(x,y,z)$ ,  $f(x_k, y_k, z_k)$  is the value of the parameter at node  $k$ , and  $x_k, y_k, z_k$  are the  $x,y,z$  coordinates of node  $k$ .

The property of these basis functions is that they sum to 1 (Huyakorn and Pinder, 1983, p. 81).

$$\sum_{k=1}^{\# \text{ nodes}} N_k = 1 \quad (8)$$

The basis functions at each node are calculated by (Huyakorn and Pinder, 1983)

$$N_k = 1/8 (1 + \xi\xi_k)(1 + \eta\eta_k)(1 + \zeta\zeta_k) \quad (9)$$

where

$\xi, \eta, \zeta$  are called isoparametric coordinates.

In this isoparametric coordinate system, the coordinates are located at the corners of a cube and have the values of  $\pm 1$  depending on the quadrant the corner is located in. Figure 18 shows the transformation of a rectangle in the  $x,y,z$  coordinate system into a cube in the isoparametric coordinate system.

So that at:

$$\text{node 1} \quad \xi_1 = -1; \eta_1 = -1; \zeta_1 = -1 \quad (10a)$$

$$2 \quad \xi_2 = 1; \eta_2 = -1; \zeta_2 = -1 \quad (10b)$$

$$3 \quad \xi_3 = 1; \eta_3 = 1; \zeta_3 = -1 \quad (10c)$$

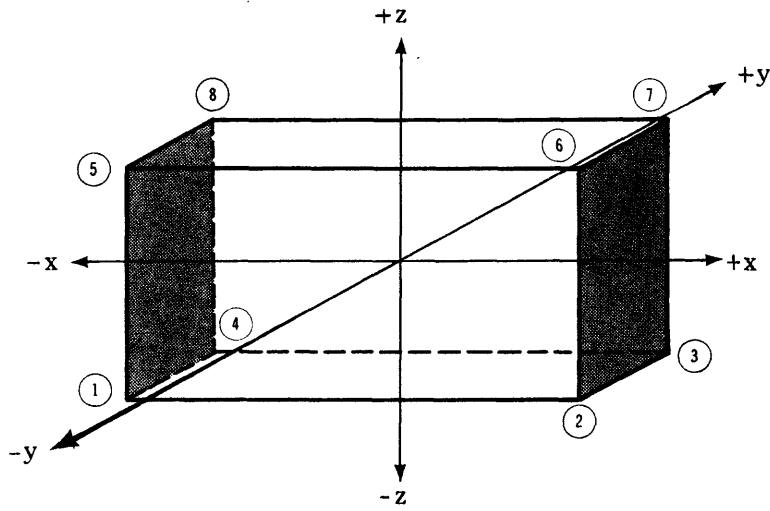
$$4 \quad \xi_4 = -1; \eta_4 = 1; \zeta_4 = -1 \quad (10d)$$

$$5 \quad \xi_5 = -1; \eta_5 = -1; \zeta_5 = 1 \quad (10e)$$

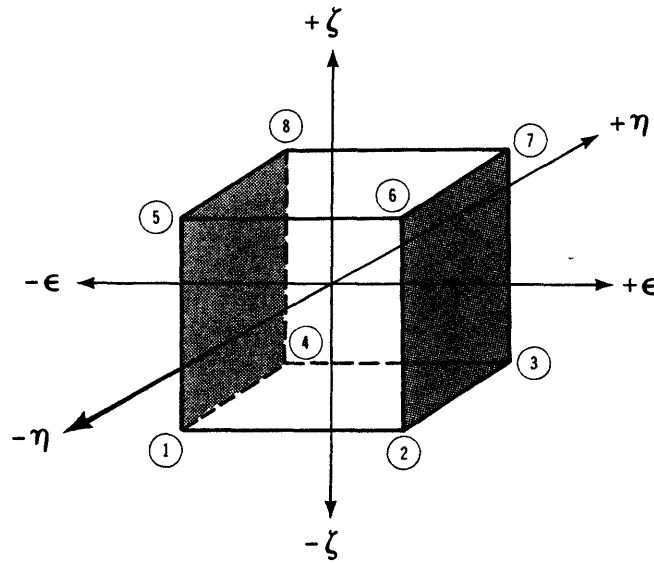
$$6 \quad \xi_6 = 1; \eta_6 = -1; \zeta_6 = 1 \quad (10f)$$

$$7 \quad \xi_7 = 1; \eta_7 = 1; \zeta_7 = 1 \quad (10g)$$

$$8 \quad \xi_8 = -1; \eta_8 = 1; \zeta_8 = 1 \quad (10h)$$



a) Finite-difference cell in  $x, y, z$  coordinate system



b) Same finite-difference cell in isoparametric coordinate system

FIGURE 18. Transformation of a rectangle in the  $x, y, z$  coordinate system into a cube in the isoparametric coordinate system.

And the equations for basis functions become

$$\text{for node 1} \quad N_1 = \frac{1}{8} (1 - \xi)(1 - \eta)(1 - \zeta) \quad (11a)$$

$$2 \quad N_2 = \frac{1}{8} (1 + \xi)(1 - \eta)(1 - \zeta) \quad (11b)$$

$$3 \quad N_3 = \frac{1}{8} (1 + \xi)(1 + \eta)(1 - \zeta) \quad (11c)$$

$$4 \quad N_4 = \frac{1}{8} (1 - \xi)(1 + \eta)(1 - \zeta) \quad (11d)$$

$$5 \quad N_5 = \frac{1}{8} (1 - \xi)(1 - \eta)(1 + \zeta) \quad (11e)$$

$$6 \quad N_6 = \frac{1}{8} (1 + \xi)(1 - \eta)(1 + \zeta) \quad (11f)$$

$$7 \quad N_7 = \frac{1}{8} (1 + \xi)(1 + \eta)(1 + \zeta) \quad (11g)$$

$$8 \quad N_8 = \frac{1}{8} (1 - \xi)(1 + \eta)(1 + \zeta) \quad (11h)$$

$(\xi, \eta, \zeta)$  are the coordinates of the particle location in the isoparametric coordinate system. The transformation from cartesian  $(x, y, z)$  coordinates to local  $(\xi, \eta, \zeta)$  coordinates is accomplished using the following equations

$$\xi = 1 - 2 * \left( \frac{x - x_1}{x_2 - x_1} \right) \quad (12a)$$

$$\eta = 1 - 2 * \left( \frac{y - y_1}{y_4 - y_1} \right) \quad (12b)$$

$$\zeta = 1 - 2 * \left( \frac{z - z_5}{z_1 - z_5} \right) \quad (12c)$$

where

$x, y$  and  $z$  are the coordinates of the parameter location in the cartesian coordinate system,

$x_2, x_1$  are the  $x$  coordinates of nodes 2 and 1,

$y_4, y_1$  are the  $y$  coordinates of nodes 4 and 1,

$z_1, z_5$  are the  $z$  coordinates of nodes 1 and 5.

With rectangular elements (finite-difference blocks)

$$x_2 - x_1 = x_3 - x_4 = x_6 - x_5 = x_7 - x_8, \quad (13a)$$

$$y_4 - y_1 = y_3 - y_2 = y_8 - y_5 = y_7 - y_6, \quad (13b)$$

$$z_1 - z_5 = z_2 - z_6 = z_3 - z_7 = z_4 - z_8, \quad (13c)$$

All coordinate differences will give the same  $\Delta x$ ,  $\Delta y$ ,  $\Delta z$ . Notice that  $\Delta z$  is calculated in the downward direction since the positive  $z$  direction is defined as being downward. The equations for the basis functions for each node evaluated at location  $x, y, z$  now become

$$N_1 = 1/8 \left\{ 1 - \left[ 1 - 2 * \left( \frac{x-x_1}{x_2-x_1} \right) \right] \right\} \left\{ 1 - \left[ 1 - 2 * \left( \frac{y-y_1}{y_4-y_1} \right) \right] \right\} \left\{ 1 - \left[ 1 - 2 * \left( \frac{z-z_5}{z_5-z_1} \right) \right] \right\} \quad (14a)$$

$$N_2 = 1/8 \left\{ 1 + \left[ 1 - 2 * \left( \frac{x-x_1}{x_2-x_1} \right) \right] \right\} \left\{ 1 - \left[ 1 - 2 * \left( \frac{y-y_1}{y_4-y_1} \right) \right] \right\} \left\{ 1 - \left[ 1 - 2 * \left( \frac{z-z_5}{z_5-z_1} \right) \right] \right\} \quad (14b)$$

$$N_3 = 1/8 \left\{ 1 + \left[ 1 - 2 * \left( \frac{x-x_1}{x_2-x_1} \right) \right] \right\} \left\{ 1 + \left[ 1 - 2 * \left( \frac{y-y_1}{y_4-y_1} \right) \right] \right\} \left\{ 1 - \left[ 1 - 2 * \left( \frac{z-z_5}{z_5-z_1} \right) \right] \right\} \quad (14c)$$

$$N_4 = 1/8 \left\{ 1 - \left[ 1 - 2 * \left( \frac{x-x_1}{x_2-x_1} \right) \right] \right\} \left\{ 1 + \left[ 1 - 2 * \left( \frac{y-y_1}{y_4-y_1} \right) \right] \right\} \left\{ 1 - \left[ 1 - 2 * \left( \frac{z-z_5}{z_5-z_1} \right) \right] \right\} \quad (14d)$$

$$N_5 = 1/8 \left\{ 1 - \left[ 1 - 2 * \left( \frac{x-x_1}{x_2-x_1} \right) \right] \right\} \left\{ 1 - \left[ 1 - 2 * \left( \frac{y-y_1}{y_4-y_1} \right) \right] \right\} \left\{ 1 + \left[ 1 - 2 * \left( \frac{z-z_5}{z_5-z_1} \right) \right] \right\} \quad (14e)$$

$$N_6 = 1/8 \left\{ 1 + \left[ 1 - 2 * \left( \frac{x-x_1}{x_2-x_1} \right) \right] \right\} \left\{ 1 - \left[ 1 - 2 * \left( \frac{y-y_1}{y_4-y_1} \right) \right] \right\} \left\{ 1 + \left[ 1 - 2 * \left( \frac{z-z_5}{z_5-z_1} \right) \right] \right\} \quad (14f)$$

$$N_7 = 1/8 \left\{ 1 + \left[ 1 - 2 * \left( \frac{x-x_1}{x_2-x_1} \right) \right] \right\} \left\{ 1 + \left[ 1 - 2 * \left( \frac{y-y_1}{y_4-y_1} \right) \right] \right\} \left\{ 1 + \left[ 1 - 2 * \left( \frac{z-z_5}{z_5-z_1} \right) \right] \right\} \quad (14g)$$

$$N_8 = 1/8 \left\{ 1 - \left[ 1 - 2 * \left( \frac{x-x_1}{x_2-x_1} \right) \right] \right\} \left\{ 1 + \left[ 1 - 2 * \left( \frac{y-y_1}{y_4-y_1} \right) \right] \right\} \left\{ 1 + \left[ 1 - 2 * \left( \frac{z-z_5}{z_5-z_1} \right) \right] \right\} \quad (14h)$$

These basis functions are then multiplied by the value of the parameter at that node according to equation 7, to give the value of that parameter at the given x,y,z location. In expanded form this becomes

$$\begin{aligned}
 f(x,y,z) = & N_1 * f(x_1,y_1,z_1) + N_2 * f(x_2,y_2,z_2) + N_3 * f(x_3,y_3,z_3) \\
 & + N_4 * f(x_4,y_4,z_4) + N_5 * f(x_5,y_5,z_5) + N_6 * f(x_6,y_6,z_6) \\
 & + N_7 * f(x_7,y_7,z_7) + N_8 * f(x_8,y_8,z_8)
 \end{aligned}
 \tag{15}$$

The x,y,z component of specific discharge can be calculated at any x,y,z coordinate using equation 15 as follows

$$\begin{aligned}
 q_x(x,y,z) = & N_1 * q_{x1} + N_2 * q_{x2} + N_3 * q_{x3} + N_4 * q_{x4} + N_5 * q_{x5} \\
 & + N_6 * q_{x6} + N_7 * q_{x7} + N_8 * q_{x8}
 \end{aligned}
 \tag{16a}$$

$$\begin{aligned}
 q_y(x,y,z) = & N_1 * q_{y1} + N_2 * q_{y2} + N_3 * q_{y3} + N_4 * q_{y4} + N_5 * q_{y5} \\
 & + N_6 * q_{y6} + N_7 * q_{y7} + N_8 * q_{y8}
 \end{aligned}
 \tag{16b}$$

$$\begin{aligned}
 q_z(x,y,z) = & N_1 * q_{z1} + N_2 * q_{z2} + N_3 * q_{z3} + N_4 * q_{z4} + N_5 * q_{z5} \\
 & + N_6 * q_{z6} + N_7 * q_{z7} + N_8 * q_{z8}
 \end{aligned}
 \tag{16c}$$

To calculate the average linear velocity, the specific discharge should be divided by the effective porosity ( $n_e$ ) of the porous media, so that

$$\bar{V}_x(x,y,z) = q_x(x,y,z)/n_e
 \tag{17a}$$

$$\bar{V}_y(x,y,z) = q_y(x,y,z)/n_e
 \tag{17b}$$

$$\bar{V}_z(x,y,z) = q_z(x,y,z)/n_e
 \tag{17c}$$

The distance a mass of water travels in a given time increment,  $\Delta t$ , may be calculated by

$$\Delta x = \Delta t * \bar{V}_x(x,y,z) \quad (18a)$$

$$\Delta y = \Delta t * \bar{V}_y(x,y,z) \quad (18b)$$

$$\Delta z = \Delta t * \bar{V}_z(x,y,z) \quad (18c)$$

The choice of the time increment,  $\Delta t$ , should be such that  $\Delta t < \Delta x/\bar{V}_x$ ,  $\Delta y/\bar{V}_y$  or  $\Delta z/\bar{V}_z$ .  
The new location becomes

$$x_{\text{new}} = x_{\text{old}} + \Delta x \quad (19a)$$

$$y_{\text{new}} = y_{\text{old}} + \Delta y \quad (19b)$$

$$z_{\text{new}} = z_{\text{old}} + \Delta z \quad (19c)$$

At this point new basis functions are evaluated at the new  $x,y,z$  location, and the procedure is repeated.